UCLouvain

FACULTE DES SCIENCES

Faculté des sciences

Mars Atmospheric CO2 clouds during the Northern Hemisphere winter

Auteur·es : Mathilde Vandevoorde
Promoteur·rices : Véronique Dehant, Ozgur Karatekin
Lecteur·rices : Viviane Pierrard, François Massonnet
Année académique 2023-2024

Acknowledgements

I would like to express my deepest gratitude to my supervisor, Ozgur Karatekin, for his unwavering support and guidance throughout the journey of this thesis. His insights and expertise have been invaluable, and his presence has been a constant source of encouragement and motivation.

Special thanks go to Orkun Teller, whose prompt and detailed responses to my numerous questions have greatly contributed to the success of this project. His explanations and suggestions have been incredibly helpful and have significantly enriched my understanding and research. I am also grateful to Ananya Krishnan for her assistance and valuable contributions. Her willingness to help and provide clarity on various aspects of this work has been greatly appreciated and has positively impacted my research. I also want to thank Véronique Dehant for helping me find this subject and for the invaluable discussions we had.

I would like to finally thank my family and my partner, Valentin, for their unwavering support during this thesis. Their love, encouragement, and understanding have been a bedrock of strength for me.

Their collective knowledge, dedication, and personal support have been instrumental in the completion of this thesis, and I am deeply thankful for their time, efforts, and enduring patience.

Contents

List of Figures

Abstract

In this study, we investigate the seasonal and interannual variability of Martian CO2 clouds, focusing on Martian Years (MY) 34, 35, and 36, corresponding to Earth dates from May 5, 2017, to December 26, 2022. Utilizing data from the Mars Climate Sounder (MCS), we analyzed over 1.19 million atmospheric profiles to explore cloud dynamics, with a particular emphasis on the northern hemisphere during winter and interannual variability. Our analysis revealed distinct patterns in cloud occurrence, altitude, and duration, influenced primarily by latitude and northern winter season. The highest concentration of clouds was observed at latitudes above 50°N, indicative of Martian winter conditions in the North Pole. Equatorial regions exhibited shorter-lived mesospheric cloud formations. interannual variability was also studied, revealing differences in cloud distribution and frequency potentially linked to atmospheric dust variations and storm activities.

1 Introduction

The study of Mars has captivated the scientific community for decades, driven by a quest to understand our planetary neighbor and the broader solar system. Figure 1 presents an array of spacecraft that have been part of humanity's endeavors to explore Mars. This fleet encompasses orbiters, landers, and rovers, each designed to contribute to our understanding of Martian geology, atmosphere, climate, and the potential for life.

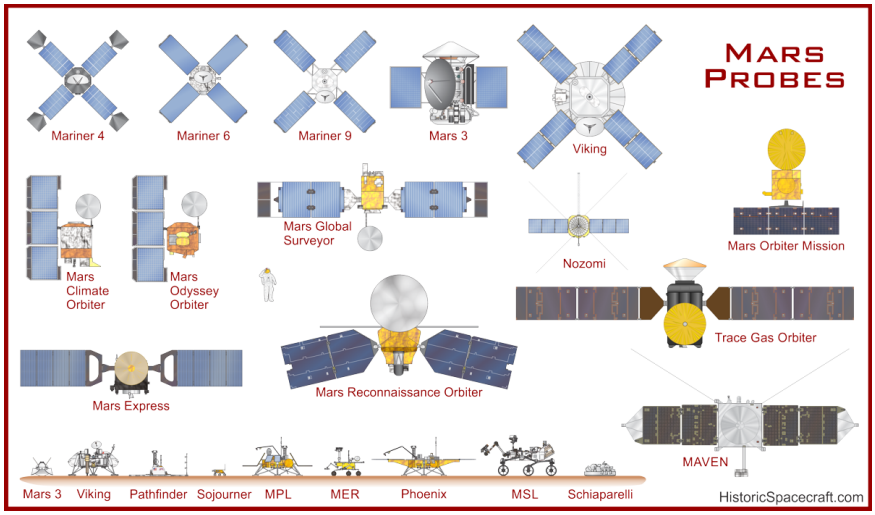

Figure 1: Summary of Mars exploration missions. Credit : historicspacecraft.com (2017) [31]

The Mariner missions were among the early flybys that provided the first close-up images of Mars. The Viking missions followed, consisting of both an orbiter and a lander, marking the first successful landing on Mars soil. The Mars Global Surveyor orbited Mars, creating a detailed map of the planet's surface, which helped identify potential landing sites for future missions. Mars Pathfinder, with its Sojourner rover, tested new technologies for deploying rovers and analyzing the Martian rocks and soil. The Mars Climate Orbiter, although unsuccessful due to a navigational error, was intended to study Mars' atmosphere and climate. [7]

The Mars Odyssey Orbiter, with its suite of scientific instruments, has been mapping the chemical elements and minerals that make up the Martian surface, providing information about the planet's geology. Mars Express, a mission by the European Space Agency (ESA), has been studying the atmosphere and surface from orbit and was intended to deploy the Beagle 2 lander, which unfortunately failed to make contact after its presumed landing. [7]

The Mars Reconnaissance Orbiter carries powerful cameras and spectrometers to further

scrutinize the surface, also serving as a vital communication relay for other missions. The Mars Exploration Rovers, Spirit and Opportunity, made groundbreaking discoveries about the past presence of water on Mars. Phoenix, another lander, studied the Martian arctic soil.

The Mars Science Laboratory, with its Curiosity rover, is a mobile laboratory determining Mars' habitability, studying its climate and geology, and collecting data for a manned mission to Mars. Nozomi was Japan's first Mars orbiter; however, it failed to enter orbit due to technical difficulties. The Mars Orbiter Mission was India first probe and was successfully launched in 2013. [11]

As outlined by the Space Study Board [52], the objectives in Martian research include several approach: firstly, "searching for evidence of past and present life" is crucial, as it may provide insights into the existence of life beyond Earth and the conditions necessary for its sustenance. Water is a fundamental criteria for terrestrial life. Despite the fact that the prevailing surface conditions on Mars are inhospitable to the stable presence of liquid water, the Martian atmosphere does contain water vapor. Additionally, when water ice comes into contact with salt, it can give rise to saline solutions, known as 'brines.' These brines can temporarily stay on the surface of Mars.[47] This objective aligns with astrobiological goals and the search for extraterrestrial life.

The second objective, "understanding the climate and volatile history of Mars", is vital for comprehending Mars' past habitability and climate dynamics. Studies have indicated that Mars once harbored liquid water and a thicker atmosphere, suggesting a climate that could have supported life. The evidence of ancient flowing and standing water, as seen in the extensive geological formations such as valley networks, river deltas, and possible oceanic bodies, corroborates the notion of a once warmer and wetter Mars. The existence of these features, especially during the late Noachian period when the Sun was fainter, poses a significant puzzle for current climate models, which struggle to replicate long-term warm conditions on early Mars. This complexity is further highlighted by the presence of widespread phyllosilicates and sulphate minerals, as detected by Mars orbiters. These minerals, indicative of aqueous alteration, suggest a history of episodic water activity rather than a consistently warm and wet climate. [50]

There is also evidence of young fluvial features, which are difficult to reconcile with the current Martian atmosphere's inability to support stable liquid water. Transient liquid water formed during the transformation of surface ice to vapor, presents a possibility for sporadic water activity on the Martian surface. The likelihood of a denser CO2 atmosphere in the past, which alone is insufficient to create a strong greenhouse effect, has led to alternative hypotheses like sulphur dioxide absorption and CO2 cloud scattering. [41]

The third objective involves "understanding geological processes and their role in shap-

ing the surface and subsurface of Mars". This aspect is key to interpreting the planet's geological history and current geologic activity, which has implications for understanding planetary evolution. Mars is well-known for its intense and frequent dust storms, ranging from small tornado-like dust devils to planet-encircling events. These storms, driven by atmospheric conditions such as wind patterns, temperature gradients, and atmospheric pressure, play a crucial role in shaping the Martian surface. [11] As these dust storms lift and redistribute vast amounts of soil and dust, they contribute to the ongoing erosion, deposition, and alteration of the Martian landscape. This constant reshaping of the surface can obscure, preserve, or reveal geological features, thereby influencing our interpretation of the planet's geological history. The intensity and frequency of dust storms are intricately tied to the Martian atmosphere. Understanding these atmospheric dynamics is essential to predict and model the occurrence of dust storms and, consequently, their effects on the Martian surface and subsurface.

Lastly, the "assessment of the nature and inventory of resources on Mars in preparation for human exploration" is a forward-looking goal.

This study focuses on analyzing and researching the Martian atmosphere by studying CO2 clouds during the Martian winter. As temperatures drop, CO2 condenses out of the atmosphere, forming clouds. These clouds are composed of ice particles of carbon dioxide, a phenomenon unique to Mars due to its thin atmosphere and cold temperatures. Unlike Earth, where clouds are primarily composed of water vapor, Mars' lower temperatures and atmospheric composition allow for CO2 to transition directly from a gaseous to a solid state, forming clouds. Studying these CO2 clouds is vital for understanding the Martian climate system. The formation, density, and distribution of these clouds can provide insights into the atmospheric dynamics, seasonal variations, and global circulation patterns on Mars. CO2 clouds play a significant role in the planet's energy balance and thermal dynamics, as they can reflect solar radiation and trap infrared radiation, affecting surface temperatures. Before delving into the specifics of this study, it is essential to review the current knowledge and research gaps in our understanding of Mars.

1.1 Characteristics of Mars

Mars, the fourth planet from the Sun in our solar system, offers a compelling arena for study, particularly due to its unique atmosphere and polar regions. Its distinct topographical characteristics and environmental conditions allow us to draw comparisons and contrasts with Earth. Much like Earth, Mars experiences seasons, a result of its axial tilt. However, these Martian seasons are markedly different from Earth's, reflecting an extreme version of Earth's seasonal variations. The Martian year, almost twice as long as Earth's, leads to more prolonged seasonal periods. Additionally, the planet experiences significant daily temperature fluctuations, with variations as high as 70 Kelvin. This extreme range is largely

attributed to Mars' thin atmosphere, which is about 100 times less dense than Earth's, failing to insulate the planet effectively. The presence of polar caps on Mars, consisting of both water ice and dry ice, further adds to the planet's intriguing environmental dynamics. These polar caps, like those on Earth, grow and recede with the changing seasons, but under conditions far more severe than those on our planet[16].

1.1.1 The orbital forcing of Mars

Mars orbits the Sun at an average distance of approximately 227.9 million kilometers. Its sidereal day is approximately 24.6 hours, making it quite similar to Earth's day-night cycle. To complete one orbit, Mars takes about 687 Earth days. Mars is smaller than Earth, with a diameter of about 6,779 kilometers, roughly half the size of our planet. Due to its smaller mass, Mars has a weaker gravitational force, about 38 % of Earth's gravity. The eccentricity, is about 0.0935 for Mars. In comparison, Earth's orbital eccentricity is about 0.0167, making Mars's orbit more elliptical. Mars' obliquity is very close to the Earth's, with a tilt of 25.19° (compared to 23.44° for the Earth). Mars thus experiences seasons like Earth, but with different duration due to its longer orbital period.

1.1.2 The atmosphere of Mars

The Martian atmosphere, is composed predominantly of carbon dioxide (95.32%), nitrogen (2.7%), and argon (1.6%), with traces of oxygen and water. You can see Mars' abudance of the major gases on Figure 2.

Mars thermal structure The planet's atmospheric pressure is less than 1% of Earth's, averaging about 6 millibars compared to Earth's 1013 millibars. This thin atmosphere, coupled with the planet's distance from the Sun, makes Mars a relatively cold planet, with average surface temperatures around 215K - 218K. Mars is a planet of extreme temperature, largely due to its thin atmosphere, which is less capable of retaining heat compared to the Earth's atmosphere. The temperature range is from 140K to 310K. Mars' atmosphere can be divided in three different layers : the lower atmosphere, the middle atmosphere and the upper atmosphere. The lower atmosphere (also called troposphere) is very similar to the Earth's troposphere : it is the closest atmospheric layer to the planet's surface and extends to about 50 km in altitude. In this layer, temperature decrease with height, as it is driven by convective and radiative tranfer. The temperature and thickness also vary greatly throughout the diurnal cycle. The middle atmosphere comprises two layers : the stratosphere and mesosphere. It goes from 50 km to 100 km, and is roughly isothermal. The upper atmosphere goes from 100 to 200 km and temperature increase with altitude. The ionosphere also begins at 100 km high and extend to 300 km above the surface. The ionosphere vary a lot with seasons. The lower and middle atmosphere will now be refered as the neutral atmosphere.

Gaseous species	Average abundance	Reference
CO_2	0.9532	Owen et al. (1977)
N_2	0.027	Owen et al. (1977)
	0.019	Mahaffy et al. (2013)
Ar	0.016	Owen et al. (1977)
	0.019	Mahaffy et al. (2013)
O_2	0.0014	Hartogh et al. (2010)
CO	800 ppm	Smith et al. (2009)
H_2O	15–1500 ppm	Smith (2004)
H_2	15 ppm	Krasnopolsky and Feldman (2001)
Ne	2.5 ppm	Owen et al. (1977)
Kr	0.3 ppm	Owen et al. (1977)
Xe	0.08 ppm	Owen et al. (1977)
O_3	10–350 ppb	Perrier et al. (2006)
H_2O_2	10–40 ppb	Encrenaz et al. (2004)
CH_4	0–40 ppb	Mumma et al. (2009)
	0.7–7 ppb	Webster et al. (2015)

Figure 2: The abundance of the major gases that make up the Mars atmosphere. The abundance of some species (notably water vapor and ozone) varies greatly with season and location. Table taken from[11].

1.1.3 Martian Atmospheric Cycles

Dust cycle Dust plays a critical role in the Martian climate system. It impacts the planet's thermal balance by absorbing, scattering, and emitting radiation, and its interactions with solar radiation drive global atmospheric circulation and weather. Mars experiences regular dust storms, which range from small whirlwinds, known as dust devils, to global dust storm. The dust in these storms primarily originates from the planet's surface, lifted either by strong winds causing wind shear or convective vortices (called dust devils) that are usually formed under strong winds, facilitated by the fact that Martian soil is composed of fine particles that are easily carried by wind. This dust then gets suspended in the atmosphere, in the Martian Planetary Boundary Layer (PBL) and can be transported long distances, influencing the planet's regional and global climate. [11] The transport and distribution of dust within the Martian PBL are heavily influenced by the diurnal and seasonal dynamics of the boundary layer. During the day, the surface heating by the Sun enhances convective activity, which can lift dust particles into the atmosphere. Studies have shown that this process can inject dust particles into the upper layers of the PBL, significantly affecting the vertical dust distribution. [44]

Mars also has a dust season, a period of the Martian year when dust storms are most

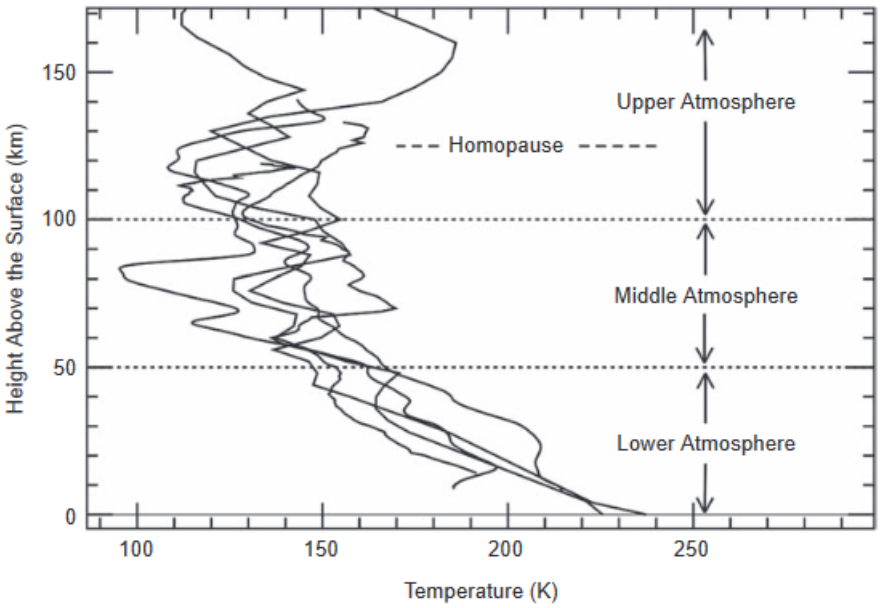

Figure 3: An overview of Mars atmosphere thermal structure, defining the "lower", "middle", and "upper" atmosphere. The temperature profiles shown are inferred from accelerometer observations during the descent through the atmosphere of landed spacecraft. [11]

likely to occur. This season coincides with Mars' perihelion (the point in its orbit closest to the Sun), which happens during the northern hemisphere's winter. During this period, the southern hemisphere is tilted towards the Sun, causing it to receive more sunlight and leading to stronger heating of the surface and atmosphere. This enhanced heating can generate large-scale winds and provoke dust storms. The dust season can lead to significant changes in the Martian atmosphere, including increased atmospheric opacity, changes in atmospheric temperature profiles, and alteration of atmospheric dynamics. These dust storms can either be global or more regional. The global dust storms happen every few years, and encompass the entire planet, drastically altering atmospheric conditions and visibility. The presence of dust can block solar radiation from reaching Mars surface leading to lower surface temperature during global dust storms.[51] On the other side, the upper part of the atmosphere will be higher in temperature, as solar radiation will be blocked by the dust, and the boundary between the neutral atmosphere and the ionosphere (the turbopause) will be higher than usual. [45]

While global dust storms on Mars are significant events that occur every few years, the planet also experiences more frequent regional dust storms annually, with their intensity and precise timing subject to variation. Mars has three different types of regional dust storm : A, B and C. They can be seen on Figure 4. The type A storm typically originate

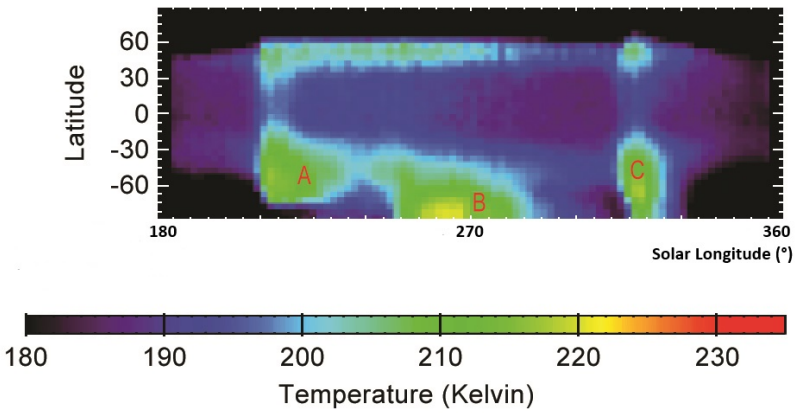

Figure 4: Martian atmospheric temperature depending on the latitude and seasons in the south hemisphere. Data collected by Mars Climate Sounder. Credit : NASA/JPL-Caltech [35]

near Mars' north pole during the northern autumn. They are similar to Earth's cold-season arctic storms that move across continents[28]. As these Martian storms move southward from the cold north hemisphere into the warmer southern hemisphere's mid-spring, the wind intensify due to the increasing temperature, resulting in much larger dust storms. The sunlight warming the dust in the atmosphere enhances wind speeds, lifting more dust and expanding the storm's area and vertical reach.

Storms classified as Type B typically emerge in the vicinity of the South Pole, coinciding with the commencement of summer in the Southern Hemisphere. They might be affected by winds created at the boundary of the retreating South Polar carbon dioxide ice cap. Such storms are known to contribute to haze in specific regions and are notably different in origin compared to Type A storms.

The last type of storms, Type C storms begin after the conclusion of the Type B storms. They originate in the north during the northern winter and migrate to the southern hemisphere, much like Type A storms. C type storms season is between 315° and 349° of solar longitude.

CO2 cycle The CO2 cycle on Mars is defined by the dynamic relationship between its atmosphere, which is predominantly made up of CO2, and the seasonal polar caps that are primarily formed from solid CO2. This cycle is significantly influenced by the seasonal variations in insolation throughout Mars' orbit around the sun. During the Martian winter, reduced insolation near the poles leads to the condensation of atmospheric CO2, forming solid CO2 at the polar caps. This process releases latent heat, partially offsetting the en-

ergy lost to space. Conversely, in warmer seasons, this solid CO2 sublimates back into the atmosphere, contributing to atmospheric pressure changes. Approximately 25-30% of the Martian atmosphere is exchanged with the polar caps annually, showcasing the significance of this cycle. [11]

The mass balance between the gaseous and solid phases of CO2 on Mars is not static but varies over longer timescales as well. Changes in Mars' orbital parameters, such as obliquity and the season of perihelion, influence the latitudinal and seasonal distribution of insolation. These changes, in turn, affect the extent and amount of seasonal CO2 ice, highlighting the dynamic nature of the Martian CO2 cycle. The seasonal condensation and sublimation of CO2 at high latitudes are vital for controlling atmospheric circulation and are therefore central to the Martian climate system. Understanding this cycle is crucial for grasping both the present and past environmental conditions of Mars. [11][24]

Water cycle On Mars, water is primarily found in solid and gaseous forms due to the planet's atmospheric conditions. This means that liquid water is rarely stable on the Martian surface. The planet's water inventory, including the atmosphere, surface ice, and the regolith (varied surface material covering solid rock, composed of dust, soil, and broken rock, mixed with water ice), is significantly less than Earth's. If all of Mars' water reservoirs were melted, they would cover the Martian surface with a water layer only 20-30 meters deep.[11] Despite its scarcity, water plays a crucial role in the Martian climate, impacting various aspects of the planet's environment.

The Martian water cycle operates in a cyclic manner, influenced by changes in the planet's orbital configuration. The patterns are controlled by exchanges between different water reservoirs, including the atmosphere, surface ice, and the regolith. The largest reservoirs are found in icy layers on the surface or mixed within the regolith, with the north polar cap being a major contributor. The Martian water cycle is dominated by the seasonal changes at the north pole, where significant amounts of water sublime from the ice cap during the spring-summer season and are injected into the atmosphere. This process is followed by extreme dryness during the polar night, when water vapor levels drop significantly. Water vapor then travels across Mars, driven by wind and atmospheric circulation, and participates in a seasonal Hadley cell that redistributes moisture between the hemispheres.

The seasonal cycle of water on Mars is a dynamic process where vast ice reservoirs interact with the atmosphere, enabling water transport from one pole to the other. This cycle is closed annually, with water vapor returning to the north during the fall-winter season to be trapped within seasonal frost. Besides sublimation and atmospheric transport, other processes like adsorption and release by the regolith, and cloud formation and precipitation, contribute to the seasonal evolution of water on Mars. [11]

Interconnection of Martian Atmospheric cycles The dust and CO2 cycles are interconnected through various processes. Dust in the atmosphere influences the amount of heat transported to the polar regions and affects the properties of seasonal CO2 ice caps. For instance, dust in the air can enhance winter CO2 condensation in the polar regions by providing condensation seed nuclei and increasing emissivity. However, the warmth from the dusty atmosphere might offset this enhancement by increasing the heat transport towards the poles. Furthermore, dust incorporated into the CO2 ice cap can change its thermal properties (like albedo and emissivity), affecting the rates of CO2 condensation and sublimation. As the wind stress that lifts dust is directly related to atmospheric mass, changes in the CO2 cycle can in turn affect the dust cycle. Martian dust cycles are marked by more intense dust events, such as regional and planet-encircling dust storms, also known as Global Dust Storms (GDS). [11]

The dust and water cycles are connected mainly through cloud condensation processes. Dust particles suspended in the atmosphere can act as seed nuclei for the formation of water ice clouds. Once dust particles are coated with ice, they fall at different speeds, changing the vertical and horizontal distribution of dust and water in the atmosphere. Additionally, these ice-covered dust particles have different radiative properties, which affect the thermal and dynamical state of the atmosphere, leading to changes in dust lifting, transportation, and sedimentation. This complex interplay between dust, water, and CO2 cycles significantly influences the current climate on Mars. [11] [48]

1.2 Mars Poles

Mars' polar regions are characterized by icy caps composed of carbon dioxide and water ice. The polar regions play a crucial role in regulating the exchange of matter between the Earth's surface and its atmosphere. Changes in the polar caps can impact atmospheric pressure, leading to variations in atmospheric circulation on a global scale. The size of the polar caps is influenced by the amount of solar radiation that reaches the surface. This radiation not only affects surface temperatures but also impacts the processes of phase change in the existing ice. The amount of solar flux received is also dependent on the planet's orbital forcing. During colder seasons, reduced sunlight exposure causes temperatures to dip, leading to the formation of solid carbon dioxide, or dry ice, which causes the polar caps to expand. In contrast, the opposite hemisphere, with increased sunlight, witnesses a reduction in dry ice, elevating the levels of gaseous CO2 in the atmosphere.

Both the North and South polar caps of Mars possess a permanent layer of water ice, approximately 3 km thick, which is overlaid by a seasonal layer of dry ice. The thickness of this dry ice layer fluctuates seasonally, ranging from none to a maximum of 2 meters. The North polar cap is 1 000 km in diameter while the south polar cap is only 400/800 km in diameter. [20]. These poles can store up to 30% of the atmospheric CO2. The North Pole

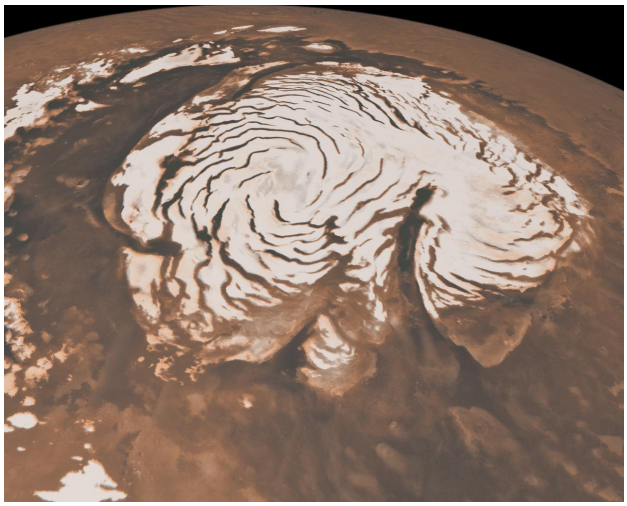

Figure 5: Northern Ice Cap of Mars. Image synthesized by Mars Global Surveyor Orbiter and Mars Orbiter Laser Altimeter data.
Credit : NASA/JPL-Caltech/MSSS

size vary depending on the season and usually goes down to 60°N in latitude in winter.

1.2.1 The surface and interior of Mars

Mars possesses a liquid inner core located at its core's heart, spanning a radius of approximately 1,500 to 2,100 kilometers, composed primarily of iron and sulfur. Enveloping the core, there exists a rocky mantle, extending across a range of 1,240 to 1,880 kilometers in thickness. Above the mantle, forming the planet's outer layer, is a crust composed of a blend of iron, magnesium, aluminum, calcium, and potassium. This outermost layer has a depth spanning between 10 to 50 kilometers. Mars currently doesn't have a global magnetic field, but there are evidence in crustal rocks for example that it used to have one earlier. This absence of a global magnetic field on Mars significantly influences the dynamics of its upper atmosphere and space weather, making it more susceptible to solar radiation and wind, which in turn affects the stability and composition of the Martian atmosphere.

Surface characteristics In this section, we will omit the ice caps completely. To understand more about them, see previous section. The average geometric albedo of Mars is 0.250 but can vary from 0.10 to 0.36 (excluding the polar caps) [4]. This variation can be explained by composition and grain size. While Mars is predominantly red, its surface displays a variety of colors, going from a reddish-ocre for the high albedo regions to grayish for the low albedo regions. Mars topography also shows a rich history. Mars is home to the largest volcano in the solar system, Olympus Mons, which stands at nearly 22 kilometers high. The Tharsis plateau, a volcanic plateau, houses several other massive volcanoes, while

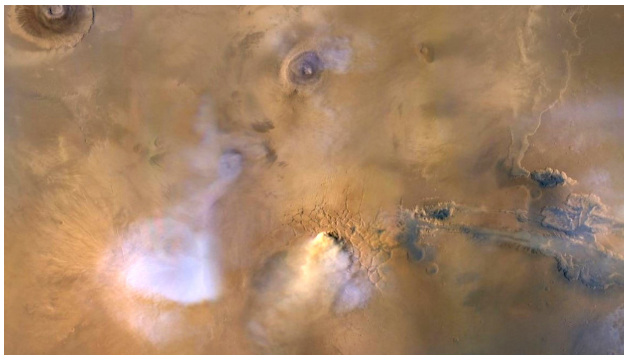

Figure 6: Image of Mars taken by MRO's MARCI. On the right is a water cloud and in the bottom-center a dust cloud that appears more yellow. Credit : NASA/JPL-Caltech/MSSS (2010) [34]

the canyon Valles Marineris is one of the most prominent features of Mars, stretching over 3,000 kilometers long and reaching depths of up to 5 kilometers. Mars is also known for its impact craters. Hellas Planitia is the largest impact basin, spanning about 2,300 kilometers in diameter and 7 kilometers deep. These variations in surface characteristics lead to differences in thermal inertia and consequently in surface temperature, which in turn influence the processes of condensation and sublimation on the Martian surface.

1.3 Mars clouds

Cloud observations on Mars have been a topic of interest since telescopes first detected them in 1877. Initially, two types of clouds were identified: yellow clouds, which were later understood to be dust storms or dust clouds, and white clouds or hazes made of either H2O or CO2 (see Figure 6).[4] These early detections laid the groundwork for more sophisticated observations. Ground-based observations continued until the significant flybys of Mariner 6 and 7 in 1969, which observed polar and detached limb hazes but could not definitively identify their composition. The Mariner 9 Orbiter in the 1970s provided the first definitive measurements of Mars' water ice cloud composition. [11]

The Viking Orbiters (1976-1982) significantly expanded our understanding of Martian cloud forms, topography, and dynamics. Their imaging data distinguished between dust and ice aerosols and revealed seasonal and spatial variability in cloud-top altitudes. Despite comprehensive atmospheric water vapor measurements by Viking's Mars Atmospheric Water Detector (MAWD), a direct correlation with water ice clouds was not immediately clear. Misinterpretations of Viking Orbiter IRTM data initially led to inaccuracies in understanding vapor saturation in Mars' atmosphere.

The resurgence of Mars exploration in the late 1990s with missions like Phobos, Pathfinder,

and Mars Global Surveyor marked a new era of investigation. These missions, along with subsequent ones like Mars Odyssey, Mars Express, MAVEN and Mars Reconnaissance Orbiter, have greatly enhanced our understanding of Martian atmospheric dust and ice aerosols through various observational techniques. Significant findings include Mars Global Surveyor Thermal Emission Spectrometer's characterization of the aphelion and polar hood cloud systems, Mars Odyssey Thermal Imaging System (THEMIS)'s interannual coverage of the aphelion cloud belt, and Mars Orbiter Laser ALtimeter (MOLA)'s detections of polar CO2 ice clouds. [11] Various instruments have supported detections of equatorial high-altitude clouds and provided insights into cloud scattering properties and particle sizes.

The recognition of the global nature of the aphelion cloud belt (ACB) and the significant roles played by Martian clouds in transport, radiation, and photochemistry emerged later, supported by Earth-based observations. These cloud-related processes have profound impacts on global and temporal variations in Mars' atmospheric temperatures, aerosols, water vapor, photochemistry, and climate evolution, prompting new modeling efforts. [40] The study of CO2 ice clouds on Mars not only sheds light on the unique meteorological phenomena of the Red Planet but also provides crucial insights into the atmospheric dynamics, thermal regulation, and perhaps even the climate evolution of Mars. The data collected so far points to a complex and dynamic Martian atmosphere, with processes and phenomena that parallel, yet are distinct from, those found on Earth. [39].

Observations indicate that Mars has clouds composed of either water ice or carbon dioxide ice. These water ice clouds show a variety of shapes, influenced by different dynamical processes. They can be observed year-round, in three distinct regions around the equator, in the south and north pole [12] and at various altitudes. Most water ice clouds on Mars form at altitudes up to 25 kilometers, often resulting from surface dust acting as condensation nuclei in supersaturated air.[17] Notably, water ice clouds can also develop at much higher altitudes, reaching 80-90 kilometers [27]. On Figure 8 are the different types of clouds found on Mars. There is a lot of variety in altitude, in season and in location.

1.3.1 Carbon dioxide clouds

Carbon dioxide clouds were first observed on the two poles on polar nights at low altitude. Later, similar clouds were discovered at higher altitudes near the equator, primarily in the spring and summer seasons. Subsequent observations identified the presence of these carbon dioxide clouds at northern mid-latitudes in the late autumn, and during the equivalent season in the southern hemisphere [40]. These clouds can have a variety of different forms, but most of them are cirrus-type, but some cumuliform clouds can also be observed, as a result of a mesospheric convection [40].

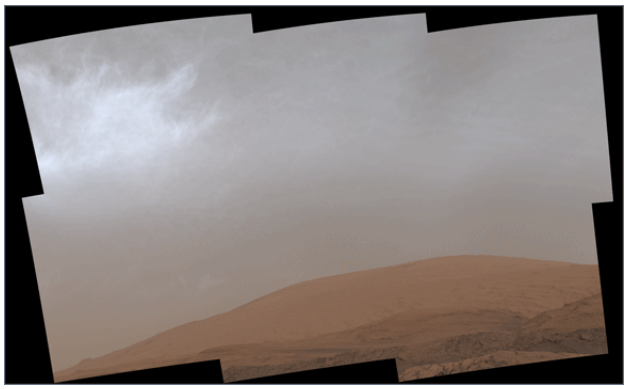

Figure 7: A CO2 mesospheric cloud over Mount Sharp captured by the rover Curiosity. Credit : NASA/JPL-Caltech/MSSS

Carbon dioxide clouds on the poles CO2 polar clouds are convective clouds. They are initiated by adiabatic ascent. During the Martian polar night, the cooling of the surface and atmosphere is balanced by latent heat from condensing CO2. This cloud formation alters the atmosphere's thermodynamics through latent heat distribution and infrared radiation scattering/absorption. Observations from various missions indicate that temperature profiles in the polar regions often follow the CO2 saturation curve up to 30 km, suggesting temperatures are buffered by CO2 condensation. Substantial cloud opacity between 0-25 km altitudes further confirm CO2 cloud formation.

CO2 clouds on Mars are unique because they form from the atmosphere's primary component, as opposed to minor elements like water vapor. The growth of these CO2 clouds is constrained solely by the release of latent heat and the self-diffusion of the gas. These clouds are typically formed through heterogeneous nucleation on surfaces like dust grains or even fine water ice particles. A supersaturation level of 35% is still required for overcoming energy barriers and initiating nucleation [13]. Polar night clouds on Mars mainly consist of ice particles affected by gravitational forces. These particles grow and sublimate as they traverse temperature variations caused by orographic gravity waves, which are influenced by local terrain features. When winds flow uphill, like over polar layered deposits, adiabatic cooling leads to the formation of large-scale clouds that are locally altered by smaller-scale gravity waves.

Carbon dioxide clouds on the equator During equatorial descents, as observed by the Pathfinder mission, CO2 has been found to exceed saturation conditions around altitudes of 80 km [43]. This suggests that CO2 cloud formation in these regions could occur at significantly higher altitudes than in polar areas. The formation of equatorial CO2 clouds is also influenced by Martian mesospheric conditions. Martian mesospheric temperatures can

fall well below the CO2 condensation point, particularly in the near-aphelion season when diurnal tides may cool CO2 down to ice cloud formation levels. Their growth is constrained by the release of latent heat and the self-diffusion of the gas. Heterogeneous nucleation, likely on surfaces like dust grains or water ice particles, is necessary for cloud formation, with a substantial supersaturation level required for overcoming energy barriers and initiating nucleation.

These high-altitude equatorial clouds exhibit dynamics influenced by Martian atmospheric tides and gravity waves. The thermal tides, particularly potent during the near-aphelion season, can create the necessary temperature conditions for CO2 ice cloud formation at these altitudes. The clouds consist of fine ice particles that grow and sublimate as they move through varying temperatures, influenced by the mesospheric wave patterns.

Carbon dioxide clouds in the sourthern hemisphere summer While not present in the Figure 8, two carbon dioxide clouds were detected recently by Jiang, Yelle et al with a solar longitude between 264° and 330°. [26] These clouds were detected above 90 km and are quite small, as their size are confined horizontally to 500 to 700 km.

Cloud type	Locations	Form	Processes	Season (L_s), LT	Spatial scale (km)	Altitude (km)	Ice	Particle R_{eff} (μm)
Global structure								
ACB	10°S–30°N	Cirrus and cumulus	Annual (eccentricity), aphelion Hadley circulation, topographic forcing	40–140°, solar tide forced variations	Global, with many cloud types listed below	10–40	H_2O	2–5
Polar hood	40–70°N,S	Cirrus, more extensive in the north	Seasonal (obliquity), wind shear and planetary eddy structure	Fall–winter, thermal tides force diurnal variations	Circumpolar haze with streak and wave cloud types	0–50	H_2O	Up to 70 below 5 km, 1–2 above 10–20 km
Polar winter CO_2	60–85°N,S	Cirrus and cumulus (?)	Lee and gravity waves, snow (?), moist convection (?)	Winter polar night	NPC topographic waves, 10–40, SPC cloud towers (?)	0–15	CO_2	10 (?)
Mid-high latitude								
NP frontal, "comma clouds"	Northern high latitudes, 50–80°N	Cirrus, frontal arcs	Polar wave systems associated with cap thermal gradients	40–110°, spring, late summer	≥500–1000 band arcs	5–30 (?)	H_2O dust	1–2 (mid-latitudes)
NP spiral	60–75°N	Cirrus spiral arcs	Polar baroclinic disturbance, anticyclonic	30–180°, repeat ~125°, morning	200–1000	10–30 (?)	H_2O	
Trough clouds	Spiral troughs in residual caps	Water ice snow?	Katabatic jump	Polar spring–summer	10–25 × 100–300	<1 (?)	H_2O	
Streaks	ACB, N and S polar hoods	Cirrus E–W linear	Strong winds, vertical shear, low temperatures	40–110° fall–winter (≥40° latitudes)	~200 (ACB) ≥500–1000 (polar hood)	10–30	H_2O	1–2 (mid-latitudes)
Streets "actinae"	ACB, NPC boundary	Cumulus 2D spacing	Free convection	100–140° NPC, spring, early fall	1–10 "cells" 100–300 long streets	10–20 (?)	H_2O	2–4 (ACB)
Lee waves	50–80°N,S, crater rims	Cirrus	Locally forced gravity waves	Spring, fall–winter	100–500, λ ~ 3–80	10–20	H_2O	
Ground fog	South basins and canyons, high latitudes	Ice haze	Cold near-surface temperatures	Night, early morning	Fills low regions	0–5	H_2O	
Volcano regions								
Central disk, with/without rays	Tharsis volcanoes and Alba Patera	Cirrus, cumulus	Upslope winds	0–180° (ACB) peak in late afternoon	Disk comparable to volcano extent, rays ~ 30×300	15–30, 5 (Alba Patera)	H_2O	2–4 (ACB)
Bore waves long clouds	Tharsis volcanoes and saddles	Cirrus	Downslope winds, "hydraulic jump"	70–140° (ACB) early morning	1000	20–25	H_2O	
Mountain lee waves	Ascraeus, Olympus Mons	Cirrus, two-tailed plume	Orographic displacement of easterly winds	Northern summer (ACB), early morning	200–500	10–25	H_2O	
Waves	Tharsis plateau	Cirrus	Wind shear instability	0–180° (ACB) morning	λ ~ 5–30	5–15	H_2O	
High altitude								
Trails	Very location-specific (10–35°S)	Cumulus, E–W linear	Forced convection peak surface heating	240–270°, early afternoon	80×500	40–50	H_2O	0.2–0.5 (also ~1.0)
Diffuse and layer hazes	50°S–50°N	Cirrus	Low temperatures	150–330°	Regional to global scale	60–110	H_2O, CO_2 (?)	0.2–1, 0.1
Equatorial CO_2	10°S–10°N, 300–360°W, 50–130°W	Cirrus, E–W oriented	Global minima in mesospheric temperatures, gravity waves (?)	0–70°, 100–160° (?), solar tide variations (?)	Thick clouds ~5–30, thin clouds ≥100	65–85	CO_2	0.5–2

Figure 8: All the types of clouds found on Mars. The table was taken from [11]

1.4 Goal and objectives of this study

This study is dedicated to the investigation of Martian cloud formations during the northern hemisphere winter and dust season. The primary data source for this research is the Mars Climate Sounder (MCS) data, renowned for its reliability and extensive coverage. The MCS provides comprehensive and longitudinal data about the Martian atmosphere, making it an ideal resource for ongoing and future studies (see Chapter 2). [18]

For a focused analysis, this study concentrates on three distinct Martian Years: MY34, MY35, and MY36, spanning from May 5, 2017, to December 26, 2022. These years were selected due to their proximity in time and the unique meteorological events they presented. MY34 was marked by a significant global dust storm [46], MY35 exhibited more typical Martian weather patterns, and MY36 was notable for a major C-type storm. These variations provide a rich basis for comparing cloud dynamics under different atmospheric conditions.

The choice to focus on the northern hemisphere winter, a period known for its dust storm activity, especially in the south pole, is particularly pertinent for studying cloud variations in relation to dust events. This approach aligns with recent research indicating a strong correlation between dust and atmospheric phenomena on Mars.

The primary objective of this study is to analyze cloud formations and durations, providing insights into the dynamics and physics of Martian clouds. A secondary objective is to explore the interannual variations among MY34, MY35, and MY36. This includes examining how dust storms impact CO2 cloud formations, given the known correlation between the Martian dust and CO2 cycles.

For this study, a custom code was developed to process and analyze the MCS data. This code was created specifically for this research and is not based on any pre-existing software.

The methodology section will introduce the MCS data and the techniques used for its collection. This will be followed by a description of the code, the presentation of the research findings, and a discussion section. The discussion will not only interpret the results but also suggest avenues for further research and potential improvements to the study's methodology.

2 Data Sets and Methods

In this section, we will present the method and data set used in this work. Different methods exists to gather atmospheric data on Mars. There are two different types of missions : the satellites use remote sensing techniques [52] while the rovers, like Perseverance or Curiosity, can gather data directly on Mars surface.[36] In this work, we will focus on the satellites and remote sensing techniques, as they enable us to achieve a much larger coverage of Mars, which is essential for our interest in vertical profiles. These profiles, which detail the variations in the planet's atmosphere from the surface to higher altitudes, are exclusively provided by remote sensing methods such as radio occultation and spectrometry.

2.1 Methodology to detect clouds

As in the atmospheric models of Mars, we make use of a method based on saturation to detect the clouds. We first need to compute the CO2 saturation temperature. We begin with the Clausius-Clapeyron equation at saturation [8] :

$$\frac{dp}{dt} = \frac{l_c}{T\delta\alpha} = \frac{l_c}{T(\alpha_{vapor} - \alpha_{condensed})}$$

where p is the pressure at saturation, l_c is the latent heat, T is the temperature at saturation and α is the specific volume. Assuming that $\alpha_{vapour} >> \alpha_{condensed}$, we have :

$$\frac{dp}{dt} = \frac{l_c}{T(\alpha_{vapor} - \alpha_{condensed})} \simeq \frac{l_c}{T\alpha_{vapor}}$$

We know from the ideal gas law that $\alpha_{vapour} = R_c T/p$, with $R_c = R/M_c$, R the gas constant and M_C the molar mass and we obtain :

$$\frac{dp}{dt} = \frac{l_c p}{R_c T^2}$$

This leads us to

$$\frac{d(\ln p)}{dt} = \frac{l_c}{R_c T^2}$$

And then

$$p(T) = p_0 \exp\left(\int_{T_0}^{T} \frac{l_c}{R_c T^2} dT\right) \simeq p_0 \exp\left(\frac{l_c}{R_c}(\frac{1}{T_0} - \frac{1}{T})\right)$$

With some algebra manipulation, we get

$$T = \frac{l_c/R_c}{l_c/(R_c T_0) - \ln(p/p_0)}$$

From this equation, we can get T_{CO2}, the saturation temperature for CO2 on Mars. We also need to take into account the fraction of Mars atmosphere that is CO2, 0.9532 [14],

and multiply the atmospheric pressure by this number to get the CO2 pressure. The next thing we need to take into account is the supersaturation level of 35%, and thus multiply p by 1.35 [15]. We then have :

$$T_{CO2} = \frac{l_c/R_c}{l_c/(R_c T_0) - \ln(1.28682 p/p_0)}$$

For CO2, $l_c = 5.9 * 10^5$ J/kg [40], $R_c = 188.922$ J/(K.kg), $T_0 = 136.3$ K, $p_0 = 100$ Pa [32]. It gives us the final equation :

$$T_{CO2} = \frac{3122.98}{22.91 - \ln(0.0128682 p)}$$

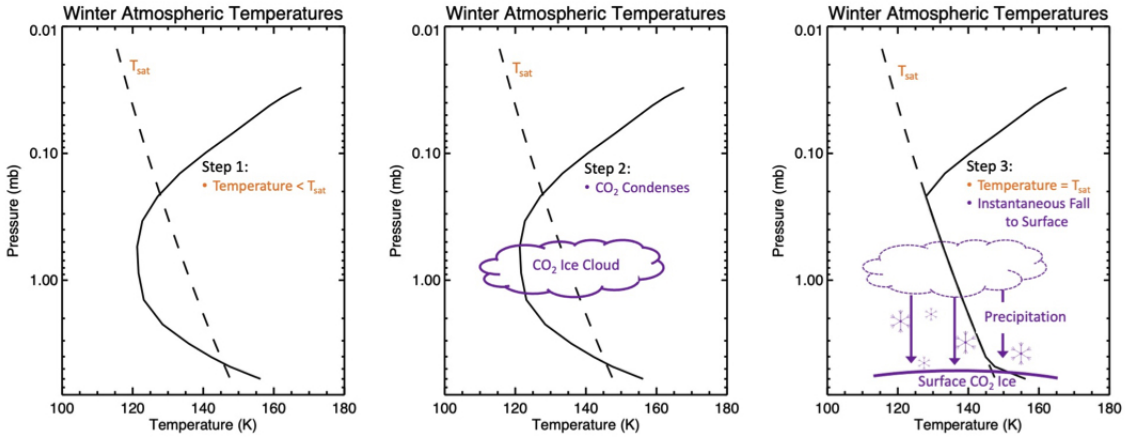

Figure 9: The formation of CO2 clouds in Mars atmosphere, as used in NASA GCM models [9]

This formula gives us the temperature at which CO2 (carbon dioxide) turns into a liquid or solid, considering the effect of supersaturation. This means that when the temperature goes below this point, the atmosphere is not able to hold the excessive amount of CO2 and thus phase change occurs as the initial point of the cloud formation process, as shown in Figure 9. The genesis of such clouds can precipitate further phenomena, namely the deposition of CO2 condensate, culminating in the formation of CO2 ice on the Martian surface.[18] We can see if this is happening by looking at graphs that show the relationship between temperature and either pressure or altitude in our data. When CO2 precipitates down and turns to ice, the air becomes less saturated with CO2. This change is reflected in our temperature and pressure readings, making them match the readings we get when the air is saturated (see 9).

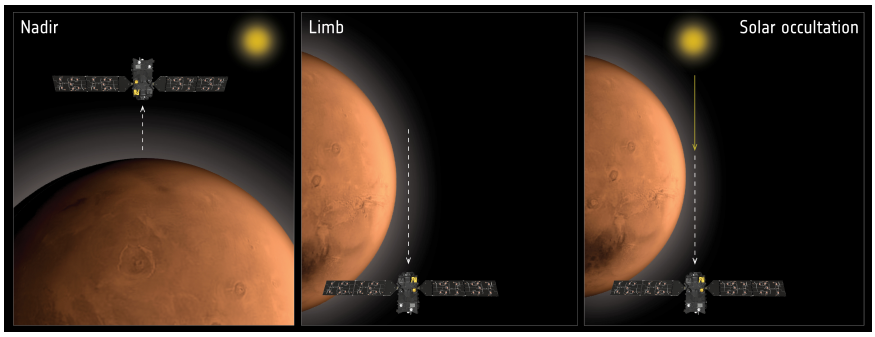

Figure 10: The difference between nadir sounding, limb staring and solar occultation. Source : ESA/ATG Medialab [38]

2.2 The instrument : MCS

MRO The MRO mission entered Mars Orbit on 10 March 2006. It is a low altitude satellite, as it orbits at 300 km from the center of Mars. The satellite got 6 different scientific instruments : three imaging systems, a visible near-infrared spectrometer, a subsurface radar, and a thermal-infrared profiler. Its mission is to observe and analyze Mars surface, subsurface and atmosphere with much higher resolution than the other satellites [52].

Eight different science investigations were chosen by NASA to gather data with the satellite. Here is an overview of all the missions. ACCEL's goal is to investigate the upper atmosphere structure using accelerometers. CRISM's (Compact Reconnaissance Imaging Spectrometer for Mars) goal is to find aqueous deposits on the surface of Mars using a spectrometer. CTX (ConTeXt Camera) is a context camera, and is used to get moderate resolution pictures of a large section of Mars. It allows MRO to get an expanded coverage. It is especially interesting as it is linked to the HiRISE (High Resolution Imaging Science Experiment) : a high resolution imaging experiment, whose goal is to take high-resolution images, but on a smaller scale than CTX. The surface pixel size is only 30 cm, and it allows scientists to have a better understanding of Mars surface. There is also the GRAVITY mission, whose goal is to study Mars gravity, as the satellite is close to the planet. The MARCI (MARs Color Imager) mission goal is to provide daily global maps of weather on Mars using one ultraviolet camera and one in the visible spectra. The SHARAD (SHallow RADar) mission's goal is to study the subsurface of Mars using a subsurface sounding radar. The last mission on board of MRO is the one we are insterested in : MCS (Mars Climate Sounder). The MCS is engineered to deliver vertical profiles of temperature, dust, and water vapor by employing remote sensing techniques that measure thermal infrared wavelengths.

MCS MCS, as a climate sounder measures changes in atmospheric temperature or composition with height. It has three different observation modes : the "in track limb staring" measures vertical profiles of temperature, pressure, aerosols and water vapor by looking tan-

gentially through the atmosphere, the "nadir sounding" measures surface infrared radiance and broadband solar reflectance by looking straight down at the atmosphere (see Figure 10) while the "polar buckshot scanning" measures the net polar radiative balance.

In this work, we will focus on the "in track limb staring". This mode involves limb scanning, where the instrument gazes sideways through the Martian atmosphere, instead of downwards as in nadir sounding. This perspective allows it to measure the vertical distribution of temperature, aerosols, and gases like water vapor across different atmospheric layers. Measurements of emissions in limb geometry involve detecting the signal emitted across a horizontal path through the atmosphere. This signal is partially absorbed during its journey from the emitting air parcel to the satellite. By changing the elevation angle of the line-of-sight (LOS), it is possible to obtain measurements of temperature and composition at different altitudes. Limb emission measurements are primarily effective in wavelengths longer than 2.5 μm, such as in the mid-infrared to microwave spectral region, due to the Planck function at terrestrial temperatures being very low for shorter wavelengths. At these longer wavelengths, atmospheric scattering is minimal, except in the presence of clouds and large aerosol particles. Unlike occultation measurements, which require a direct illumination source, emission measurements can be taken during both day and night.

These measurements can provide global coverage with dense spatial distribution, depending on the satellite's orbit, and the azimuth angle can be chosen freely as long as it avoids direct sunlight. However, the emission technique has a lower signal-to-noise ratio compared to occultation measurements, due to the weak nature of atmospheric emissions, especially on Mars given the thin atmosphere. Accurate calibration and precise determination of the LOS elevation angle are essential to prevent errors in the calculated trace gas abundance profiles. The key to this mode is the understanding of radiative transfer in the Martian atmosphere. As the instrument detects infrared emissions, it can deduce the temperature and composition based on the intensity and wavelength of the radiation.[37]

Figure 11 presents the spatial coverage of MCS over 24 hours on Mars, as MRO travels around the planet. This satellite allows us to have observations even on the Poles. MCS has been gathering data since it's launch in 2006, and hasn't stopped since. The gathering is daily. The observation strategy aims to minimize gaps in limb sounding. However, due to Mars' aspheric shape and the orbital eccentricity of the MRO, latitude-dependent adjustments are necessary for precise limb-staring observations.[37]

The MCS use a filter radiometer, and uses 9 different channels to gather data. Each with a unique function, such as measuring temperature at various altitudes or detecting dust. Its spectral range is 0.3 to 45 μm and it has two identical telescopes. The optical bench is capable of articulating in two axes, permitting both limb and nadir viewing. This feature provides a 270° range of motion in both azimuth and elevation axes, ensuring complete

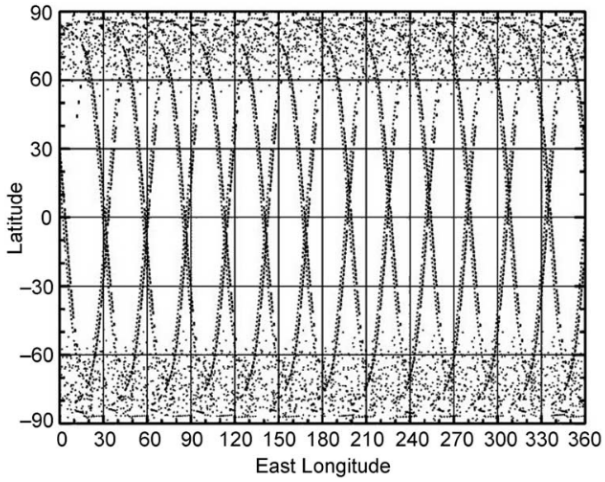

Figure 11: Mercator projection of 24 hours of MCS spatial coverage. Image taken from [37].

hemispheric coverage beneath the payload platform oriented towards the nadir.[37]

Each of the MCS telescopes consists of a mirror assembly and a focal plane structure, all supported within the optical bench by a metering structure. Despite being identical in design, the telescopes differ in their focal planes. Telescope A is equipped with six spectral channels, ranging from visible to mid-infrared wavelengths. These channels utilize optical interference filters positioned over thermopile detector arrays. Conversely, Telescope B includes three far-infrared spectral channels, defined by conductive mesh filters over the detector arrays. The nominal Field of View (FOV) response of these detectors, aligns meticulously with the filters and spectral channel assignments against the Martian limb. In this work, the data used come from telescope A first three spectral channels and telescope B three channels. [37]

In terms of optical design, both telescopes are off-axis, all-reflective, and telecentric, featuring 4 cm apertures and 4.3° FOVs. The system is composed of three mirrors, with the secondary mirror establishing the instrument aperture. The tertiary mirror, in tandem with band-pass filters and baffles, focuses an f/1.7 beam onto the focal plane detectors. The baffles, crucially positioned, serve dual purposes: acting as light pipes for the detectors and reducing the FOV response wings, thereby enhancing measurement accuracy.

The telescope mirrors, crafted from diamond-turned nickel-plated aluminum, are post-polished to diminish scattering at visible wavelengths. Their surfaces are coated with silicon dioxide-protected aluminum, optimizing reflectivity across both visible and infrared wavelengths. The metering structure, apart from supporting the mirrors, also incorporates internal baffles that shield the space between the tertiary mirror and the focal plane.

Figure 12: The MCS flight instrument photographed during calibration. Major elements are identified. Image taken from [37]

Thermal stability is paramount for the unchopped radiometer design of the MCS. To combat potential thermal drifts, especially given the day-night temperature contrasts on Mars, the design maximizes the thermal mass of the telescope and enhances thermal conductivity between its components. Conductive isolation of the telescopes from the optical bench is achieved using fiberglass washers, effectively insulating them from environmental heat variations. The optical bench, regulated in temperature, serves as a stable thermal environment for the telescopes and focal planes, ensuring minimal thermal distortion in alignment.

The spectral passbands of the MCS are defined by individual spectral filters mounted in front of each of the nine detector arrays. Telescope A's mid-infrared filters span an 11.8 to 22.2 μm range, made from Germanium substrates for their mechanical robustness and high optical transmission. Telescope B's far-infrared filters consist of stacks of mesh filters developed by Cardiff University. The thermal stability of these filters is critical, as they respond to a wide range of wavelengths and any temperature fluctuations can significantly impact the measurements.

To further refine the accuracy, the filter assemblies throughout the MCS incorporate aluminum alloy baffles. These are strategically positioned between the detectors and the filters to curtail the transmission of off-axis rays, a result of reflections within the assemblies and from the detector surfaces. The precision of these baffles, combined with their anodized coating, effectively reduces off-axis reflections, thereby contributing to the MCS's high-resolution atmospheric measurement capabilities. MCS data is downloadable online at this adress : `https://atmos.nmsu.edu/PDS/data/`. MCS data also has errors, but it wasn't included in this study.

2.3 Radio occultation data

In this work, while radio occultation has not been directly employed, it's important to recognize its potential applicability and utility for future studies. Radio occultation involves the transmission of radio waves between spacecraft or between a spacecraft and a ground station. This technique, though not utilized in our current research, can be easily integrated into our existing code framework for enhanced atmospheric analysis. Understanding radio occultation and the capabilities of various satellites currently orbiting Mars is crucial, as they provide a wealth of data that could significantly enrich future investigations into Martian atmospheric phenomena.

Radio occultation (see Figure 10) is a method used in planetary science to study the Martian atmosphere. This technique involves the transmission of radio waves between two spacecraft or one spacecraft and a ground station on Earth, with one usually orbiting Mars. As these radio waves pass through Mars atmosphere, they are refracted depending on the atmospheric conditions such as density, temperature, and pressure. By measuring the extent of this refraction, these atmospheric conditions can be derived back. This includes data on temperature gradients, atmospheric pressure at various altitudes, and the overall density of the atmosphere. This method is particularly effective for constructing vertical profiles of the Martian atmosphere, offering insights into different layers and helping understand the atmospheric dynamics of Mars. Radio occultation is advantageous for Martian exploration for several reasons. It provides high-resolution data that is crucial for understanding the Martian climate, including seasonal variations and atmospheric phenomena. This technique is robust and reliable, capable of delivering accurate measurements even during challenging conditions like dust storms, which can hinder other observational methods.

There are currently several satellites orbiting around Mars gathering data about the atmosphere. We will provide a concise overview of each satellite currently orbiting Mars. Mars Odyssey was launched in 2001 and is still used to this day.[42] The mission's objective is to create the first comprehensive map showing the quantity and spatial distribution of various chemical elements and minerals composing the surface of Mars using spectrometers. It is the longest lasting spacecraft on Mars.

Another satellite orbiting around Mars is the Mars Reconnaissance Orbiter, also called MRO. The data we use in this work comes from one of MRO's instruments : Mars Climate Sounder. MCS data has already been used in the study of clouds on Mars (see [5] or [18] for example). No study has been done globally and focused on one season. Further informations about MRO and MCS will be given.

The Mars Atmosphere Volatile EvolutioN (MAVEN) mission is a NASA spacecraft that was launched on 18 november 2013.[49] It's purpose is to measure the composition and

structure of the ionosphere and the upper atmosphere. The spacecraft entered Mars orbit on 21 september 2014, but the ROSE experiment began in July 2016. The spacecraft include a radio occultation instrument, the Radio Occultation Science Experiment (ROSE). It allows MAVEN to make atmospheric profiles of Mars.

Another spacecraft also uses radio occultation : Mars Express. It is the European Space Agency first mission to Mars, and it was launched in 2003. The main objectives of Mars Express are to study the Martian atmosphere and climate, the planet's structure, mineralogy, geology, and to search for traces of water. It carries eight instruments for these purposes, including the MaRS Radio Science Experiment. [10]

Additionally, the ExoMars Trace Gas Orbiter is operational, representing a collaborative effort between the European Space Agency and Roscosmos, the Russian space agency. Launched in 2016, its primary mission is the investigation of methane and other trace gases in the Martian atmosphere. [30] The Emirates Mars Mission, under the aegis of the United Arab Emirates Space Agency, along with China National Space Administration's Tianwen 1, are two more recent additions to Mars exploration, both having embarked on their journeys in 2020.

2.4 Code

For this work, a user friendly, open-access Python 3.0 code was developed to analyze the data. The custom code use Jupyter Notebook. This code was created specifically for this research. It uses the python routine developed by H. Sert (ROB) for MCS data reading. The code is not based on any pre-existing software. The code downloads the data from the MRO website for MY34, 35 and 36 and sorts them to only keep the data in winter, corresponding to a solar longitude L_s between 270 and 360°. When the data is sorted, for each profile, the code extracts every information that is needed : temperature at different altitudes, pressure at these altitudes, the altitudes, the date, the time, the latitude, the longitude and the L_s of the profile.

When the code has all these information, it can check whether a cloud is detected or not using the formula discussed earlier. A cloud is detected whenever the atmospheric falls below the saturation temperature of CO2. It is also capable of determining cloud precipitation by examining the temperature curve and verifying its alignment with the CO2 saturation temperature.

After this is done, the code analyzes every cloud are assembles them into what we will call in this work a "cloud event" on Figure 9. Cloud events will be the term used in this work to refer to an assembly of different profiles referring to the same cloud. Since we have profiles every minute, and since clouds can last a few hours, the same cloud will be

detected on several profiles. The code thus determines "cloud events" which are related to one cloud, and allows us to know key data like duration or the maximum/minimum altitude of the cloud. Similarly, "precipitation events" are defined in the same way but focus on precipitation. A cloud that is precipitating is still categorized as a cloud within the context of a cloud event.

After this, the code gives us several different graphs and maps depending on the data analysis requirements. The code is accessible online on GitHub at this link :
`https://github.com/MathildeVandevoorde/Extract_MRO`.

3 Results

3.1 Data coverage

For this study, we chose to focus on three different Martian Years : Martian year 34, 35 and 36. It corresponds to dates going from 5 May 2017 to 26 December 2022. These three Martian years exhibit different atmospheric dust variations. Therefore, investigating each of them provides us a chance to understand the inter-annual variability of the Martian CO2 clouds. On Figure 13 is the zonal means of the daily dust present in the atmosphere. Mars Year 34 is known for a big dust storm in between a solar longitude of 180° to 300°, and a smaller one from 330° to 350°. Mars Year 35 exhibited a relatively lower atmospheric dust opacity compared to the other two. Mars Year 36 was also different, because it had a bigger C-type storm than the two other years.

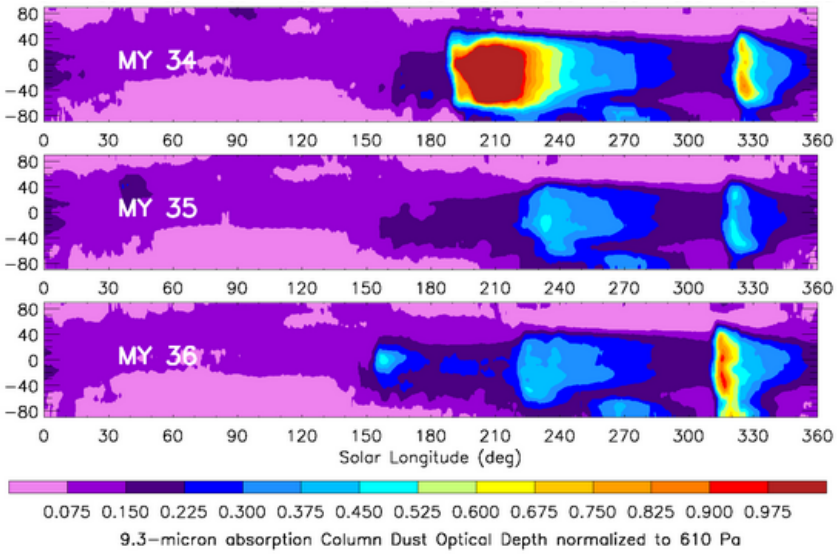

Figure 13: Zonal means of the daily regularly kriged maps of 9.3 μm absorption column dust optical depth normalized to the reference 610 Pa pressure level for the different Martian Years. Image taken from [33]

We only focused on data with a solar longitude (L_s) between 270° and 360°, corresponding to the winter in the northern hemisphere and dust storm season. The data analyzed is represented in Figure 14. We can see that the data has a good spatial coverage : the points corresponding to each profiles we studied cover the whole planet. We can also see the trajectory of MRO, given in Figure 11. Except for this criteria, we used all the data from MCS for these years. It allows us to have 323 046 different profiles in MY34, 475 454 in MY35 and 396 301 in MY36. We thus have in total over a million (1 194 801) different events analyzed.

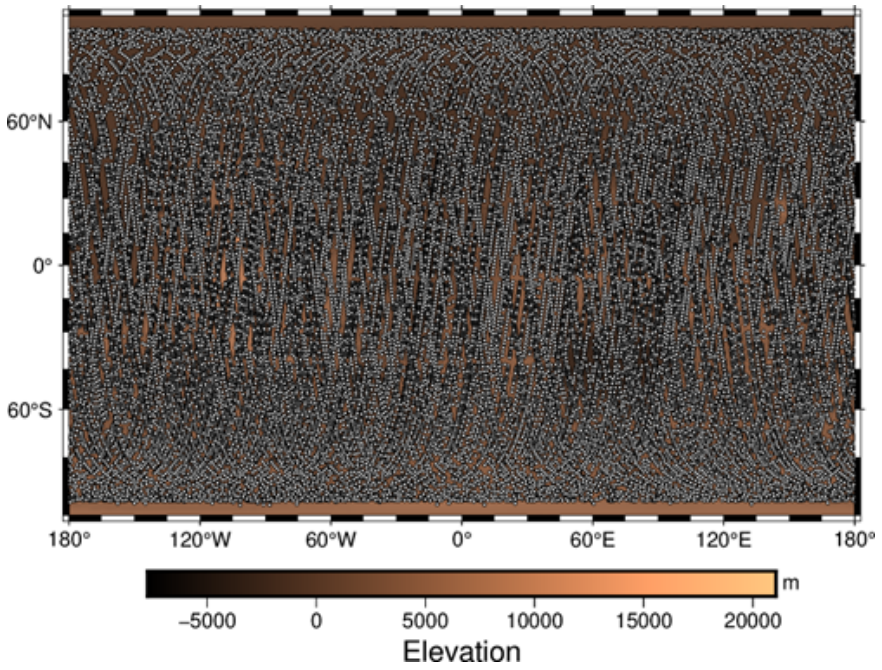

Figure 14: The data analyzed. Each point corresponds to one profile.

3.2 Temperature and CO2 clouds formation

On Figure 15 a plot is shown where a cloud and precipitation were detected. The first graph was made using data from 24/10/2022 at 06:13AM local hours with a latitude of 84° and longitude of 102°. It detected a cloud formation in the atmosphere, distinctly visible between approximately 100 Pa and 10 Pa. This pressure range corresponds to an altitude of about 10 km to 30 km. At these altitudes, the temperature falls below the CO2 saturation temperature, leading to the atmosphere's inability to retain excess CO2, resulting in cloud formation. The second graph represents data from the same day but at 06:51 AM, and at a different location with a latitude of 85° and longitude of 8°. Despite similar altitudes and pressures, the graph's profile significantly differs from the first. It runs parallel an really close to the saturation curve, indicating that the cloud is precipitating. As the cloud precipitates, the air become less saturated by CO2, thus resulting in this kind of graph. This a typical result given by our analysis. It allows us to see the cloud easily and when it precipitates also. This cloud is located on the North Pole with a latitude of 84.696°N and was taken on 24/10/2022 at 6 AM. This corresponds to a solar longitude of 326°. This cloud lasted about 3 hours, with periods of precipitation intermittently followed by periods without any precipitation. There are also a lot of profiles without any CO2 clouds detected as on Figure 16. It is in fact the majority of the profiles analyzed, with 102,977 different profiles being identified with a cloud and more than 900 000 without.

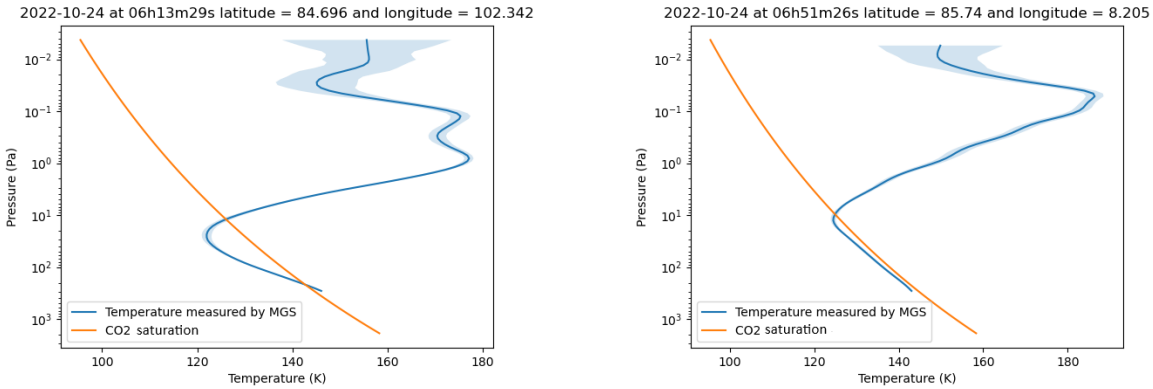

(a) A cloud

(b) A precipitation

Figure 15: Temperature vs Pressure graph of Mars atmosphere on 24/10/2022 at 06 AM made by the code.

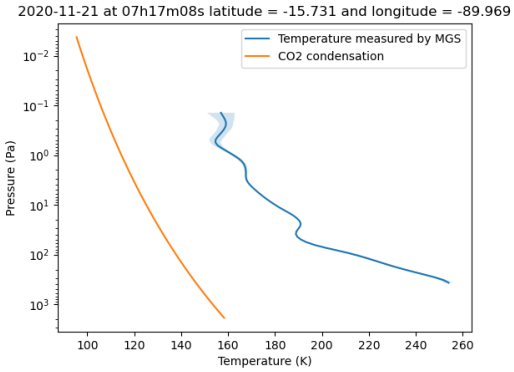

Figure 16: Temperature vs Pressure graph of Mars atmosphere on 21/11/2020 at 07 AM.

The code can also provide altitude vs temperature profiles. Let's analyze one "cloud event" completely, shown on Figure 17. On November 28 2022 the code detected a cloud at 05:24 AM at latitude 83.9° and longitude 129.3°. The cloud was detected at approximately 20 km high in the atmosphere. The cloud stays approximately the same for one hour, and as you can see on Figure 17 is still there at 06:20. At 06:21, the cloud start to precipitates and then disappear at 06:40. This is a typical cloud on the North Pole in winter, as we will see in the next section.

Another interesting cloud event to analyze is a completely different one because it happens on the equator and not in the north pole on December 25th 2022. On Figure 18 are different cloud events located on the equator. The first graph (a) is taken at 02:24 with a latitude of 1.154°N and a longitude of 113.899°E. A cloud is detected 57 km high in the atmosphere.

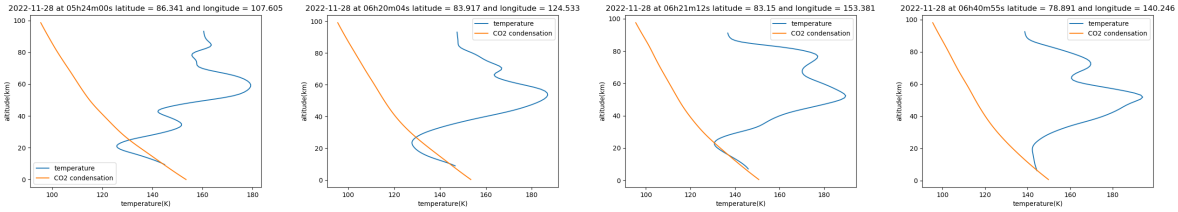

(a) at 05:24 (b) at 06:20 (c) at 06:21 (d) 06:40

Figure 17: Temperature vs Altitude graphs taken on 2022-11-28.

The second graph (b) was taken at 02:25 with a latitude of 2.672°N and -113.693°E. No cloud can be seen. The same can be said with the two last graphs on Figure 18 (c) and (d) : the third one was taken at 02:27, 15.4°N and -111.9°E, while the fourth was taken at 02:28, 16.9°N and -112.4°E. The clouds on the equator do not last long.

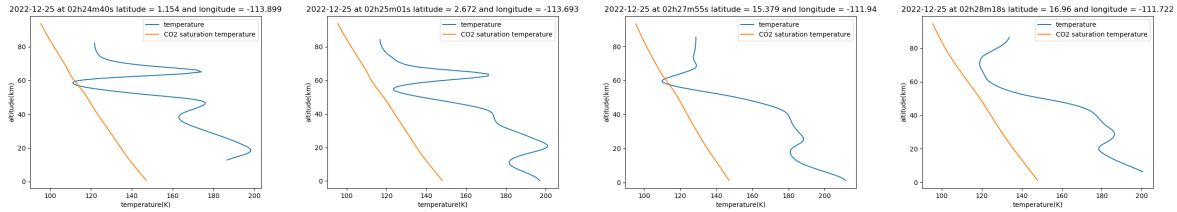

(a) at 02:24 (b) at 02:25 (c) at 02:27 (d) at 02:28

Figure 18: Temperature vs Altitude graphs taken on 2022-12-25.

3.3 Cloud occurrence

Here we will be talking about the "cloud events" (assemblies of different profiles referring to the same cloud), as mentioned in the Methodology to detect clouds section. 28 764 different cloud events were detected by the code, with or without precipitation. The first interesting thing to study is the appearance of CO2 clouds depending on the coordinates. We have on Figure 19 the same map as in Figure 14, but with only the points where a CO2 cloud was detected. The first interesting thing to notice are the latitudes : the majority of the points seems to have a latitude of 50°N or higher, in the North Pole. This is due to the season chosen, as it is winter in the North Pole and summer in the South Pole. A little less than 300 clouds have been detected on the equator, with a latitude between 20°N and 20°S.

Three clouds have also been detected in the South hemisphere. These may be authentic cloud formations, especially considering the recent findings of mesospheric CO2 clouds during the summer of the southern hemisphere, as indicated in the research [26]. Remarkably, these three clouds share similar solar longitudes (332°, 344°, and 325°), suggesting a seasonal occurrence. This pattern aligns with the recent findings of Jiang, Yelle, and others [26]. Two of these clouds were observed in Martian Year (MY) 35 and one in MY36, implying that such clouds are recurring annually, not just isolated incidents. They appear briefly, and although their temperatures are slightly above the CO2 saturation point, they remain near this critical threshold. Two clouds were detected at exceptionally low altitudes (300m and 800m), which, during the storm season, raises the possibility of them being false positives, potentially caused by atmospheric dust affecting ground temperatures. The third cloud, found at a much higher altitude of 80 km, is more likely to be a genuine cloud formation. Given the extensive data collected, it is clear that such clouds are rare and infrequent occurrences.

On Figure 20 is the type of event detected. The event "cloud" is when a cloud is detected but doesn't precipitate, while the event "precipitation" is when a CO2 precipitation happens after a cloud was formed (see Figure 9). Precipitation events happen in a line between 40°N and 80°N. There also seem to be precipitation almost only on the North Pole, and not on the Equator, as we expect, since clouds on the Equator should be mesospheric clouds and thus not precipitate.

On Figure 21, you can see the maximum altitude of the clouds. This can help us to identify clouds in the lower or in the middle atmosphere. The obvious information here is that the majority of the clouds are located in the lower atmosphere and between 0 to 30 km. These clouds are all in the North atmosphere, and are located above 40°N. There are also a lot of clouds from 30 to 60 km high. These clouds are located, for the majority, on the North Pole, so above 60°N. Some of them are also located on the equator. The majority of the clouds with the highest altitudes, from 60 to 90 km high, also called mesospheric clouds, are

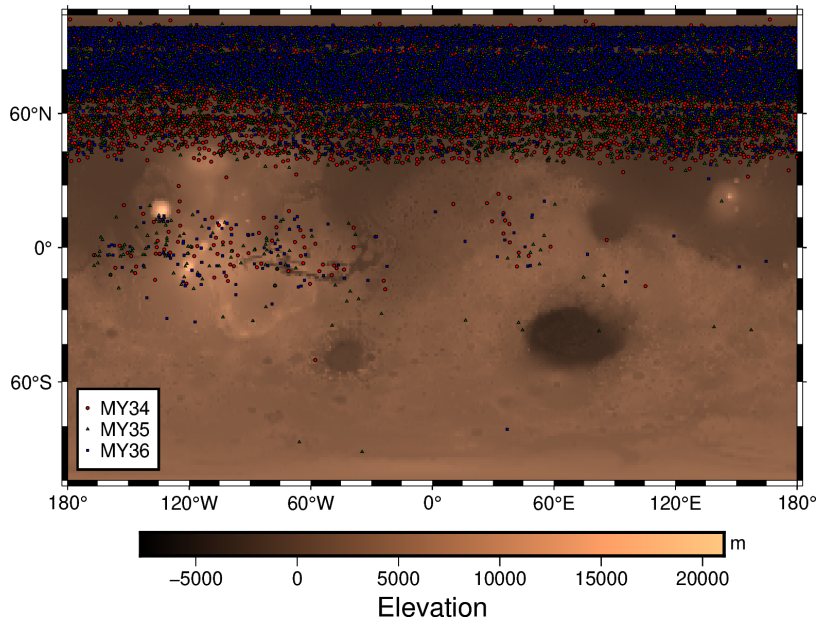

Figure 19: The clouds detected by our code. Each point corresponds to one profile where a cloud was detected. In red are the points detected in Martian Year 34, in green Martian Year 35 and in blue Martian Year 36.

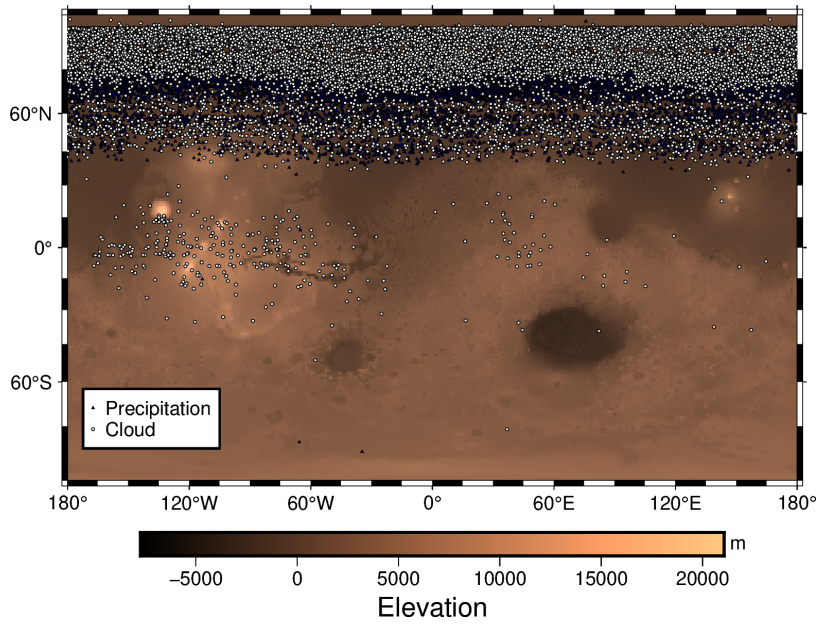

Figure 20: The clouds detected by our analysis. Each point corresponds to one profile where a cloud was detected. In white are the clouds detected and in blue the CO2 precipitations.

located between 20°N and 20°S, on the equator.A significant concentration of these clouds is also observed longitudinally between 170°W and 30°W. This area encompasses notable Martian landmarks such as the Tharsis Montes, Mons Olympus and the Valles Marineris. This region is characterized by its relatively higher altitude compared to other Martian areas. The elevated altitude results in lower atmospheric pressure, which in turn facilitates cloud formation.

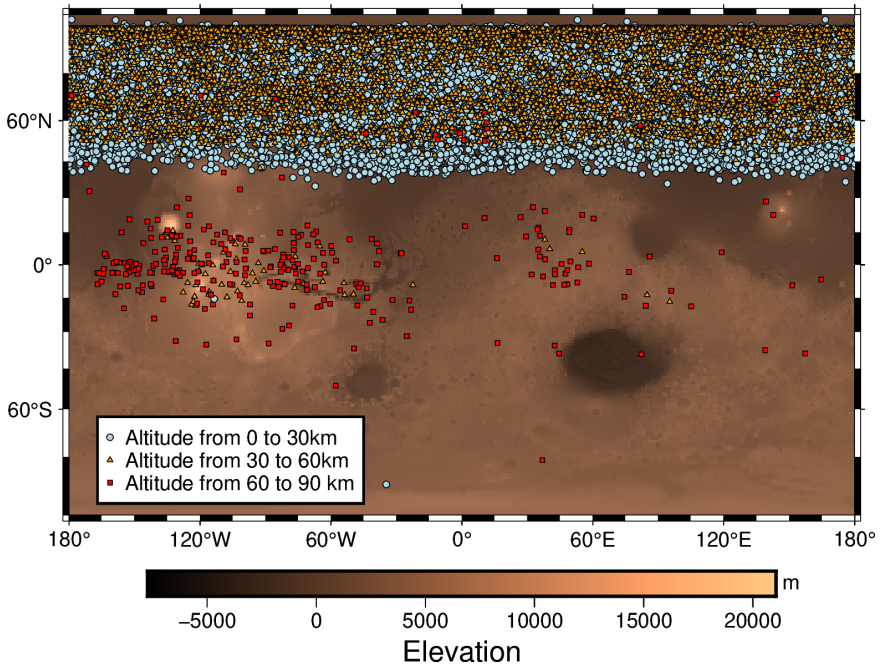

Figure 21: The clouds detected in our study. Each point corresponds to one profile where a cloud was detected. In blue are the clouds with a maximum altitude from 0 to 30 km up, in orange 30 to 60km and in red 60 to 90km.

Figure 22 illustrates the duration of cloud formations. It is observed that all clouds located at the equator have a duration of less than 30 minutes. In contrast, clouds at the North Pole (regions above 60°N) exhibit a unique characteristic, being the only ones that can persist for more than 4 hours. Additionally, the North Pole displays a versatile range of cloud durations, spanning from just a few minutes up to 4 hours. Conversely, clouds situated below the 60°N boundary typically last between a few minutes and a maximum of 3 hours.

An interesting observation is the local time when the clouds are detected. On Figure 23 is the distribution of cloud events based on the initial time of cloud formation. Clouds seems to form majorly in the interval between 2 AM and 5 AM, but there is also a lot of clouds forming between 10 AM and 3 PM. However, this observation should be considered in the context of data uniformity. On Figure 23 (a) is the distribution of cloud events based on the initial time while on (b) is the distribution of all profiles, encompassing both cloud events

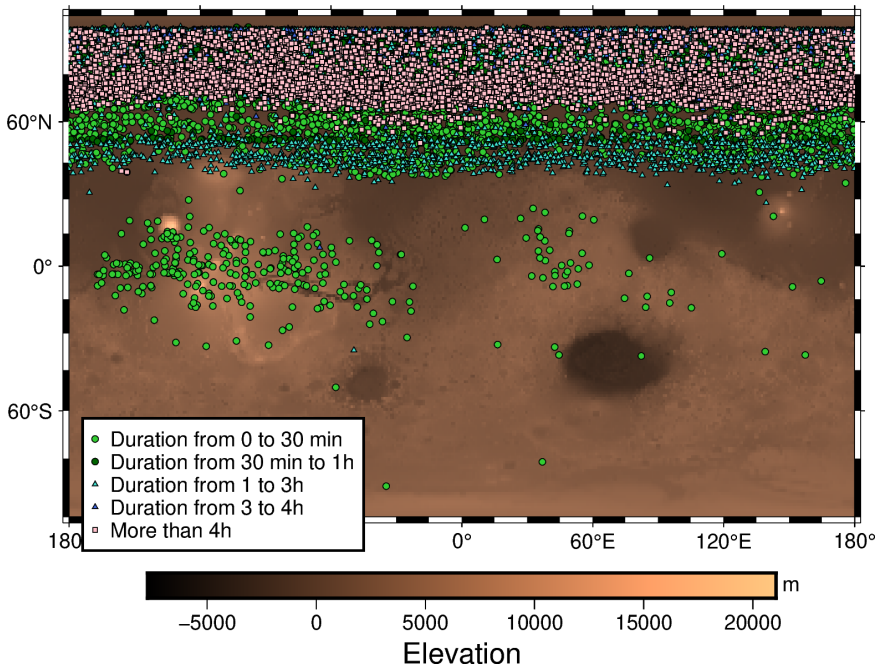

Figure 22: The clouds detected in our study. Each point corresponds to one profile where a cloud was detected. The clouds color and forms vary depending on the cloud duration.

and instances where no clouds were detected. Given the non-uniform nature of the data, our graph in part (a) may not precisely indicate the peak times for cloud formation. That's why Figure 24 was also made, as it is the distribution of cloud events based on the initial time normalized by the distribution of all profiles. This gives us totally different information about the initial formation time, as the clouds seem to form mainly between 3AM and 13PM, with the peak at 11AM and 12AM.

The variation in cloud formation timing at the Martian North Pole during winter may be influenced by data bias. Given that the North Pole remains predominantly dark in winter without sunlight, theoretically, there should not be the observed time-based differences in cloud formation as depicted in Figure 24. The non-uniform nature of the data collection could also contribute to these variations. Specifically, certain hours might have such sparse data that it becomes challenging to draw statistically significant conclusions. Therefore, the observed diurnal variations in cloud formation could be more reflective of the data collection inconsistencies rather than actual atmospheric phenomena.

We have identified three distinct types of clouds: mesospheric CO2 clouds located at the equator and in higher altitude regions, which are short-lived; a range of clouds at the North Pole, varying in altitude but generally lasting longer; and clouds in the Southern Hemisphere that are found at either very low or very high altitudes. Additionally, our findings indicate

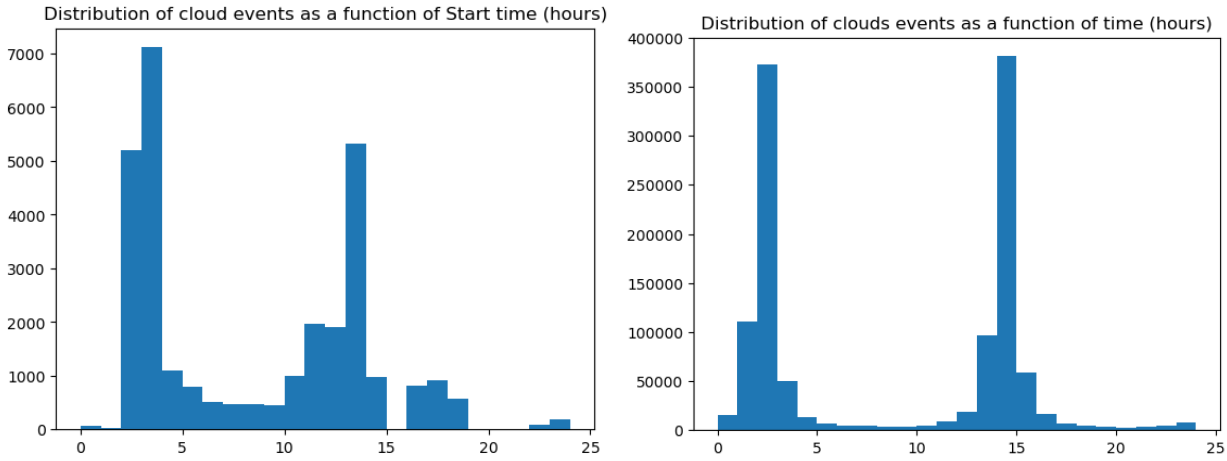

(a) Distribution of cloud events based on the initial local time of cloud formation

(b) Distribution of data based on local time when the profiles were taken.

Figure 23: Distribution of events based on time (in hours).

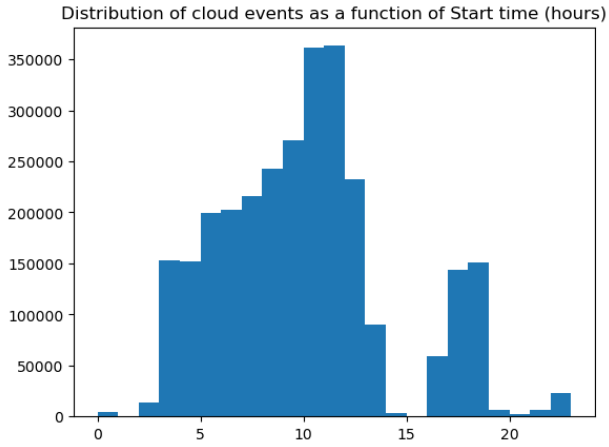

Figure 24: Distribution of cloud events based on local time (in hours) normalized with the data. Each bin was divided by the number of data for this bin and multiplied by the total number of data.

that precipitation occurs exclusively at the North Pole.

3.4 Interannual variations

Let's start by analyzing interannual variations on the poles. In Figure 25, the clouds detected for each year are presented separately, facilitating a clearer comparison of the differences. There appears to be no significant variation in the quantity of clouds between Mars Years

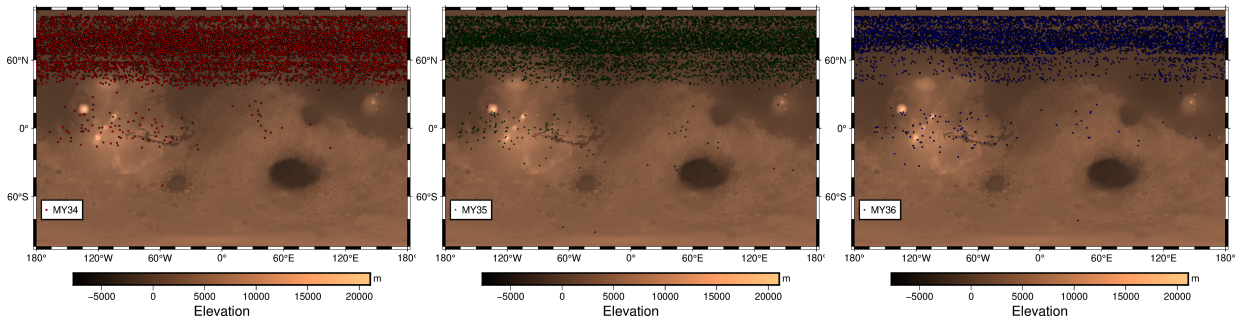

(a) Mars Year 34 (b) Mars Year 35 (c) Mars Year 36

Figure 25: The clouds detected by our code. Each point corresponds to one profile where a cloud was detected. In red are the points detected in Martian Year 34, in green Martian Year 35 and in blue Martian Year 36.

(MY) 34, 35, and 36. Specifically, there were 9,319 detected cloud events in MY34 (for 323 046 profiles), 11,023 in MY35 (for 475 454 profiles), and 8,422 in MY36 (for 396301 profiles). This can be rationalized in comparison with the data we have for each year: 2.885% for MY34, 2.318% for MY35, and 2.125% for MY36. In MY35 and MY36, there is a noticeable boundary at 60°N, above which there is a higher concentration of clouds than below. In contrast, the clouds in MY34 are more evenly distributed spatially, as this distinct difference is not visible. On Mars, interannual changes in the atmosphere are almost always due to dust, and as Mars Year 34 is known for a big dust storm, we can expect that this difference is due to it.

Another difference that can be seen is in Mars Year 36. The phenomenon seem to be the opposite of Mars Year 34, as the data seem to be much less spatially distributed and confined on top of the 60°N boundary. This year experienced a larger C-type storm than MY34 and MY35, suggesting a potential correlation. However, without data from additional years, it's challenging to draw definitive conclusions. There does not seem to be any difference in the equatorial clouds between the years.

It is also interesting to analyze the difference in data and cloud events depending on L_s for each year. On Figure26 are the distribution of the data depending on the solar longitude. Unfortunately, there is not any data for Mars Year 34 between 270° and 280° from MCS. The dataset does not have any data for this period. The distribution in data is not totally uniform, as it seems they are more data at the end of winter than at the beginning for the three years.

The distribution of cloud events can be seen on Figure 27, the clouds seem to increase while reaching the end of the year. This is due to the fact that there is more data for the

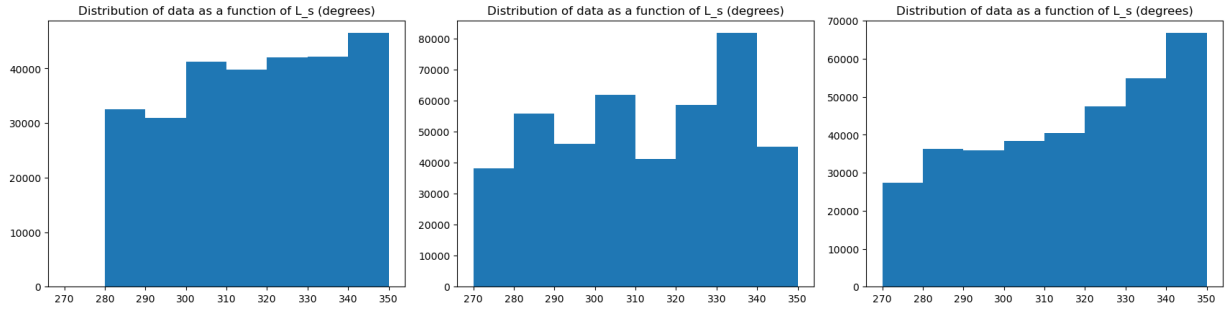

(a) Mars Year 34 (b) Mars Year 35 (c) Mars Year 36

Figure 26: Distribution of data depending on the solar longitude.

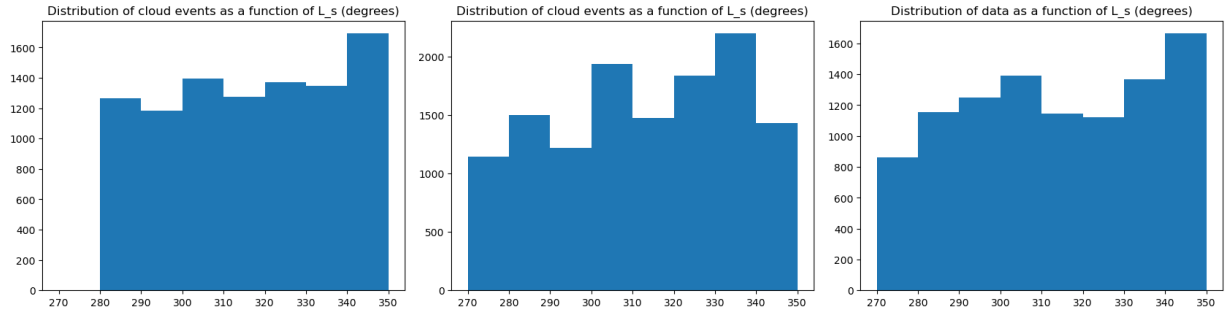

(a) Mars Year 34 (b) Mars Year 35 (c) Mars Year 36

Figure 27: Distribution of cloud events depending on the solar longitude.

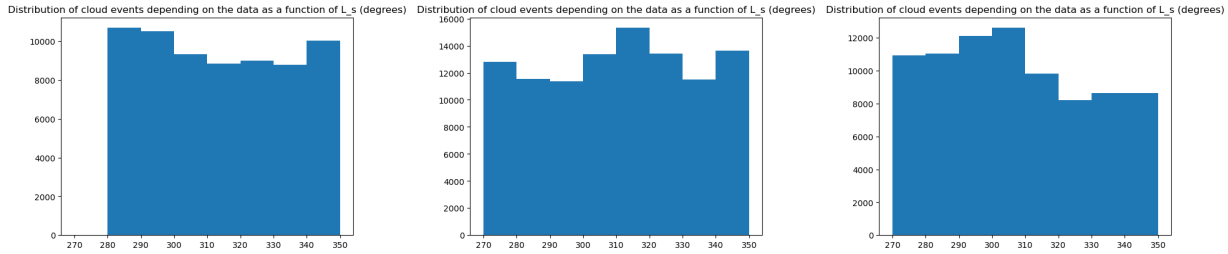

(a) Mars Year 34 (b) Mars Year 35 (c) Mars Year 36

Figure 28: Distribution of cloud events depending on the data and on the solar longitude. Each bin was divided by the data number for this bin and multiplied by the total number of data for each year.

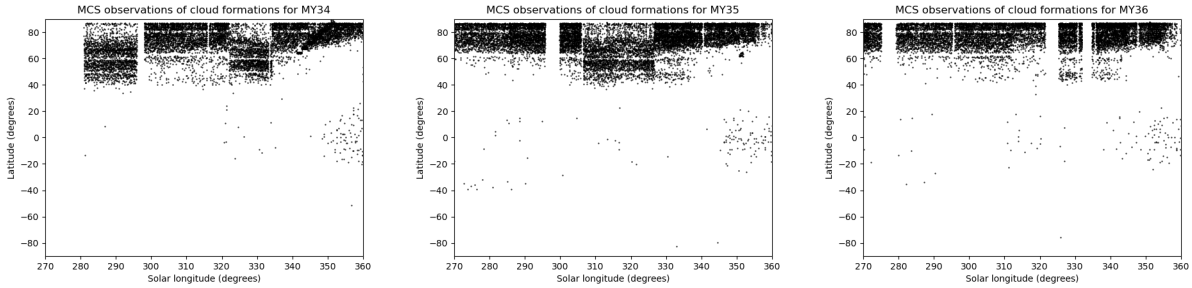

(a) Mars Year 34 (b) Mars Year 35 (c) Mars Year 36

Figure 29: Distribution of cloud events across Solar Longitude. Each point corresponds to one profile where a cloud was detected.

end of each year as seen on Figure 26. Due to the nonlinear nature of the data, Figure 28 illustrates the distribution of cloud events relative to the solar longitude. Each bin is normalized by the count of data points it contains, and then scaled by the annual total data count to enhance visibility on the graph, especially since the original values were fractional. This gives us a way to have the information we need about the difference in each year of cloud appearance depending on solar longitude. Mars Year 34 seem to have a lot of clouds at the beginning of winter, corresponding to the end of the global dust storm, and also has a lot of clouds at the end of winter, while the appearance of clouds in the middle of winter seem to be almost constant. For Mars Year 35, there are a lot of clouds in the middle of the winter, and also a bit more than usual at the beginning and at the end. For Mars Year 36, there is a visible difference between the end of winter and the beginning. The lowest bar corresponds exactly to the C-storm season, and as the C-storm this year was bigger than the other years this could explain it. If we look at the other two years, there is also less clouds in the C-storm season (315° to 349°), indicating a correlation.

Figure 29 illustrates the distribution of cloud formations as a function of solar longitude for Martian Years 34, 35, and 36. Notably, cloud formations at the North Pole are visible each year, as the winter season ends the number of clouds decreases toward Ls 360. The cloud distribution show some interannual variations. During the early winter of MY34, there's an observable expansion of cloud coverage to broader areas, a trend also evident at the end of the C-type storm season (solar longitude from 315° to 349°), with clouds extending to 40°N. Outside of these periods, clouds typically are not detected below 60°N. In MY35, there's a noticeable increase in cloud persistence, especially below 60°N during the C-type storm season. MY36, marked by a significant C-type storm, shows an even greater persistence of clouds, predominantly above 60°N. However, during the C-type storm season, a slight increase in cloud formations is observed below 60°N, though these are less extensive compared to the previous two years

Figure 29 additionally provides insights into the equatorial mesospheric clouds, which predominantly appear towards the end of winter, with a solar longitude ranging from 340 to 360° over the three observed Martian Years. In MY34, the majority of equatorial clouds are observed at year's end, hinting at a potential link with the global dust storm happening at the beginning of winter. For MY35, these clouds are present throughout the winter, but there is a noticeable increase towards the season's end. In contrast, MY36 shows a higher frequency of equatorial clouds during both the C-type storm season and the latter part of the year.

Our observations suggest an increased amount of clouds while there was a global dust storm. This correlation may be attributed to the lower temperatures typically found in the lower atmosphere during such storms, as discussed in Section 1, which likely promote cloud formation. Conversely, C-type storms tend to result in a decrease in cloud formation, especially during larger storms. However, there is an observed increase in cloud coverage area, which is more pronounced when the C-type storms are smaller in scale. This phenomenon may be explained by the geographic occurrence of most clouds, which are predominantly observed at the northern pole, and the fact that C-type regional storms generally do not extend beyond 40°N in latitude.

4 Discussion and Further Perspectives

In this study of Martian cloud dynamics, particularly focusing on the northern hemisphere during the winter seasons of Martian Years 34, 35, and 36, we have gained insights into the atmospheric dynamics of Mars. The analysis of over 1 million different events revealed that the highest concentration of clouds occurred at latitudes above 50°N, correlating with the winter season in the Martian North Pole. The equatorial region also showed mesospheric cloud formation. This pattern underscores the influence of seasonal and latitudinal factors on cloud formation on Mars. The detection of clouds in the Southern Hemisphere presents an intriguing area for further research, especially considering they have only been observed once previously [26].

The study's detailed examination of cloud events revealed important characteristics about Martian cloud dynamics. For instance, clouds at the equator are short-lived, typically lasting less than 30 minutes, while those at the North Pole can persist for more than 4 hours, exhibiting a diverse range of duration. The analysis of cloud formations based on local time showed a predominant formation period between 2 AM and 5 AM, with another significant period between 4 AM and 1 PM. Our findings showed that the diurnal meteorological variations can drive the cloud formation processes.

Additionally, the interannual comparison across the three Martian Years did not reveal a consistent pattern in cloud appearance relative to solar longitude except for the C-type storm season and global dust storm suggesting complex interactions between atmospheric conditions and dust storm activities. The significant drop in cloud events during the C-storms further highlights the impact of dust storms on Martian cloud dynamics, and might be attributed to the geographic occurrences of most clouds. The increased amount of clouds during the global dust storm may be attributed to the lower temperature in the atmosphere due to the dust. The changes in cloud coverage over the years, especially during the C-type storm season, further suggest interactions between dust and clouds. These findings not only enhance our understanding of Martian atmospheric phenomena but also lay the groundwork for future research, particularly in modeling atmospheric conditions on Mars.

We have successfully developed a method to read and analyze Mars Climate Sounder (MCS) data obtained directly from an online publicly available dataset. While there exists a substantial body of literature focusing on MCS data, most of these studies have not concentrated specifically on the analysis of Martian clouds in the northern hemisphere winter. This is particularly true for the more recent Martian Years (MY) 34, 35, and 36.

My work stands out as it globally analyzes cloud formations during the winter season in Mars' northern hemisphere. Given that Martian Years 34, 35, and 36 are relatively recent, there exists a significant gap in the comprehensive analysis of these periods, especially MY

36. By focusing on these years, this works study the interannual variation of the atmospheric behavior and cloud patterns of Mars.

This analysis contributes to a better understanding of Martian meteorology, particularly cloud dynamics and their seasonal and interannual variations. The findings of this study also provide a basis for future research on Mars' climate, potentially aiding in the planning of future Mars missions. Thus, this study offers a new perspective on Martian clouds, particularly in the context of recent Martian years and specific seasonal patterns.

This analysis is fundamentally a statistical one, executed automatically by a numerical code and analysis. Given the sheer volume of events under consideration, manual analysis was impossible. This enormity inevitably implies the possibility of false detection and errors within the data. However, it is important to note that we detected more than 28,000 cloud events. These false detection, while present, are likely to be a small fraction of the total detection and thus do not significantly detract from the overall validity and reliability of the findings.

The scale of data allowed for a robust statistical approach, ensuring that the overall trends and patterns identified are representative of the actual atmospheric conditions on Mars, despite the potential minor inaccuracies. Moreover, while manual analysis was impossible for all the data, a smaller sample was tested manually, enhancing the confidence in the results and in the code.

As previously mentioned, the Mars Reconnaissance Orbiter (MRO) is in constant motion, completing a full orbit around Mars roughly every 2 hours. This unique orbit allows it to cover the entire Martian surface within a single day. However, this extensive coverage also means that observations made even minutes apart are not conducted at the exact same geographical coordinates in terms of latitude and longitude. Consequently, our code and analytical methods, while adept at identifying cloud formations, encounter limitations in tracking these clouds over time. Specifically, if a cloud is not spatially extensive, our system may detect it at one point but fail to do so in subsequent observations.

This phenomenon is exemplified in Figure 18, where two distinct events are presented. Here, the inability to consecutively track the same cloud formation across different time frames becomes apparent. Due to the rapid movement of the MRO and the variable nature of cloud formations, it becomes challenging to determine whether certain clouds dissipate quickly or are simply too small to be detected in consecutive measurements. Therefore, while our methodology is robust in identifying cloud presence, it encounters inherent limitations in assessing the duration and persistence of these clouds.

Another limitation associated with the movement of the Mars Reconnaissance Orbiter

(MRO) is the potential amalgamation of multiple cloud formations into a single 'cloud event' by our analytical code. The code is designed to operate in the following manner: if a cloud is detected in multiple consecutive profiles, the system classifies this as a single cloud event. While this approach is effective in many cases, it encounters a specific problem due to the orbital motion of the MRO. As MRO traverses the Martian skies, it could encounter two distinct cloud formations located in close proximity to each other. Given the code's methodology, there is a possibility that these separate cloud entities could be erroneously identified as a single event. This issue is not just a technicality but has broader implications for our understanding of Martian cloud dynamics. Accurately distinguishing between individual cloud formations is crucial for a detailed analysis of cloud duration. This can lead to, in areas where cloud are prolific, really long clouds, as seen on Figure 22.

Therefore, while our code provides a tool for detecting and analyzing Martian cloud events, this aspect underscores the need for enhanced algorithms or additional observational strategies. Such improvements would enable more precise differentiation between closely spaced cloud formations.

Expanding the scope of this study to include additional Martian seasons beyond winter would improve our understanding of the planet's atmospheric dynamics. This comparative analysis would provide insights into the planet's meteorological processes, revealing how cloud behavior and atmospheric conditions vary from season to season. For instance, analyzing Martian Year 34 during the global dust storm would be particularly intriguing. In this study, we only analyzed the latter part of it, as the storm began in the fall. Moreover, extending the temporal range of the study by incorporating data from more Martian years would allow for a more nuanced understanding of inter-annual variability in cloud formations. This long-term data could unveil patterns and trends that are not apparent in shorter study periods, and allow us to confirm our hypotheses. It may provide insights into the stability and variability of Martian climate over extended periods, enabling a better understanding of Martian meteorology and its potential evolution over time. It would also help to determine if the clouds detected by our analysis in the southern hemisphere were false positives or genuine cloud formations.

Another improvement lies in diversifying the data sources. Utilizing data from other satellites or Mars rovers would offer a different observational perspective, potentially uncovering nuances or phenomena that the Mars Climate Sounder (MCS) might miss. This approach is particularly important in remote sensing, where instrumentation and observational biases can skew data interpretation. By comparing MCS data with that from other sources, we can validate the accuracy of our findings and identify any biases or limitations inherent in the MCS data. For instance, cross-referencing our data collected via spectrometry with that obtained through radio occultation can provide insights into the potential limitations or inaccuracies of the spectrometer.

Cross-referencing our observations with established models like the Mars Climate Database (MCD) or other Martian Global Circulation Models (GCMs) could also be done. This comparison serves a dual purpose: it not only assesses the accuracy and reliability of these models but also offers insights to refine and enhance them. By aligning our empirical data with these models, we can identify discrepancies and areas for improvement.

An important future direction for this research involves refining the existing code to enable the identification of water ice (H2O) clouds on Mars. While our current focus has been predominantly on the detection and analysis of Martian CO2 clouds, the expansion to include H2O clouds is a crucial step. This addition would allow for a study of the distribution, frequency, and characteristics of H2O clouds, and their interaction with other atmospheric phenomena on Mars. Understanding the behavior of both CO2 and H2O clouds is vital, as it contributes to a more holistic view of Martian atmospheric dynamics.

Incorporating the analysis of H2O clouds into our research will also significantly enhance our understanding of the Martian hydrological cycle. This is particularly important given the implications of water ice clouds in the context of potential past or present life on Mars, as well as for future human exploration. By studying these clouds, we can gain insights into the seasonal and perhaps even diurnal variations of water vapor and ice in the Martian atmosphere. This could provide information about the planet's past climatic conditions and its capacity to support life, even in microbial forms.

Moreover, this expanded focus will enable a more detailed examination of the Martian climate and weather systems. Understanding the dynamics of H2O clouds in relation to CO2 clouds can reveal much about the temperature, pressure, and atmospheric composition variations on Mars. By expanding our research to include the study of H2O clouds on Mars, we will not only enhance the comprehensiveness of our study but also contribute insights into the Martian hydrological cycle, climatic conditions, and atmospheric dynamics. This approach will enrich our overall knowledge of the planet's atmosphere and could have far-reaching implications for both Martian and terrestrial atmospheric sciences.

The code was shared to other researchers and is accessible online to everyone. By making the code accessible to others, it enables scientists to analyze MCS data in their own studies. This widespread use can lead to a variety of insights and findings about the Martian atmosphere. The ability of the code to process and analyze MCS data means that researchers can now delve into more detailed and specific aspects of Mars' atmospheric conditions. This could include studies on atmospheric composition, temperature variations, wind patterns, and seasonal changes, among others.

References

[1] Nasa planetary fact sheet. `https://solarsystem.nasa.gov/resources/681/solar-system-temperatures/`. Accessed : 09-07-2023.

[2] *The Geology of Mars: Evidence from Earth-Based Analogs*. Cambridge Planetary Science. Cambridge University Press, 2007.

[3] S. Aoki, Y. Sato, M. Giuranna, P. Wolkenberg, T.M. Sato, H. Nakagawa, and Y. Kasaba. Mesospheric co2 ice clouds on mars observed by planetary fourier spectrometer onboard mars express. *Icarus*, 302:175–190, 2018.

[4] Nadine Barlow. *Mars: An Introduction to its Interior, Surface and Atmosphere*. Cambridge Planetary Science. Cambridge University Press, 2008.

[5] Jennifer L. Benson, David M. Kass, and Armin Kleinböhl. Mars' north polar hood as observed by the mars climate sounder. *Journal of Geophysical Research: Planets*, 116(E3), 2011.

[6] W.M. Calvin, B.A. Cantor, and P.B. James. Interannual and seasonal changes in the south seasonal polar cap of mars: Observations from my 28-31 using marci. *Icarus*, 292:144–153, 2017.

[7] Michael H. Carr. *Overview*, page 1–22. Cambridge Planetary Science. Cambridge University Press, 2007.

[8] David C. Catling. Chapter 16 - mars atmosphere: History and surface interactions. In Tilman Spohn, Doris Breuer, and Torrence V. Johnson, editors, *Encyclopedia of the Solar System (Third Edition)*, pages 343–357. Elsevier, Boston, third edition edition, 2014.

[9] Mars Climate Modeling Center. Gcm overview: Lecture, November 2021.

[10] A. Chicarro, P. Martin, and R. Trautner. The Mars Express mission: an overview. In Andrew Wilson and Agustin Chicarro, editors, *Mars Express: the Scientific Payload*, volume 1240 of *ESA Special Publication*, pages 3–13, August 2004.

[11] R. Todd Clancy, Franck Montmessin, Jennifer Benson, Frank Daerden, Anthony Colaprete, and Michael J. Wolff. *Mars Clouds*, page 76–105. Cambridge Planetary Science. Cambridge University Press, 2017.

[12] R. Todd Clancy, Michael J. Wolff, Barbara A. Whitney, Bruce A. Cantor, and Michael D. Smith. Mars equatorial mesospheric clouds: Global occurrence and physical properties from mars global surveyor thermal emission spectrometer and mars orbiter camera limb observations. *Journal of Geophysical Research: Planets*, 112(E4), 2007.

[13] Anthony Colaprete, Jeffrey R. Barnes, Robert M. Haberle, and Franck Montmessin. Co2 clouds, cape and convection on mars: Observations and general circulation modeling. *Planetary and Space Science*, 56(2):150–180, 2008. Mars Polar Processes: Atmosphere-Surface Interactions.

[14] M. Giuranna, D. Grassi, V. Formisano, L. Montabone, F. Forget, and L. Zasova. Pfs/mex observations of the condensing co2 south polar cap of mars. *Icarus*, 197(2):386–402, 2008.

[15] David L. Glandorf, Anthony Colaprete, Margaret A. Tolbert, and Owen B. Toon. Co2 snow on mars and early earth: Experimental constraints. *Icarus*, 160(1):66–72, 2002.

[16] Robert M. Haberle, Manoj M. Joshi, James R. Murphy, Jeffrey R. Barnes, John T. Schofield, Greg Wilson, Miguel Lopez-Valverde, Jeffery L. Hollingsworth, Alison F. C. Bridger, and James Schaeffer. General circulation model simulations of the mars pathfinder atmospheric structure investigation/meteorology data. *Journal of Geophysical Research: Planets*, 104(E4):8957–8974, 1999.

[17] V. L. Hartwick, O. B. Toon, and N. G. Heavens. High-altitude water ice cloud formation on mars controlled by interplanetary dust particles. *Nature Geoscience*, 12(7):516–521, Jul 2019.

[18] Paul O. Hayne, David A. Paige, John T. Schofield, David M. Kass, Armin Kleinböhl, Nicholas G. Heavens, and Daniel J. McCleese. Carbon dioxide snow clouds on mars: South polar winter observations by the mars climate sounder. *Journal of Geophysical Research: Planets*, 117(E8), 2012.

[19] Renyu Hu, Kerri Cahoy, and Maria T. Zuber. Mars atmospheric co2 condensation above the north and south poles as revealed by radio occultation, climate sounder, and laser ranging observations. *Journal of Geophysical Research: Planets*, 117(E7), 2012.

[20] Christine S. Hvidberg. *6 Polar Caps*, pages 129–153. Springer Berlin Heidelberg, Berlin, Heidelberg, 2005.

[21] Takeshi Imamura, Hiroki Ando, Silvia Tellmann, Martin Pätzold, Bernd Häusler, Atsushi Yamazaki, Takao M. Sato, Katsuyuki Noguchi, Yoshifumi Futaana, Janusz Oschlisniok, Sanjay Limaye, R. K. Choudhary, Yasuhiro Murata, Hiroshi Takeuchi, Chikako Hirose, Tsutomu Ichikawa, Tomoaki Toda, Atsushi Tomiki, Takumi Abe, Zen-ichi Yamamoto, Hirotomo Noda, Takahiro Iwata, Shin-ya Murakami, Takehiko Satoh, Tetsuya Fukuhara, Kazunori Ogohara, Ko-ichiro Sugiyama, Hiroki Kashimura, Shoko Ohtsuki, Seiko Takagi, Yukio Yamamoto, Naru Hirata, George L. Hashimoto, Manabu Yamada, Makoto Suzuki, Nobuaki Ishii, Tomoko Hayashiyama, Yeon Joo Lee, and Masato Nakamura. Initial performance of the radio occultation experiment in the venus orbiter mission akatsuki. *Earth, Planets and Space*, 69(1):137, Oct 2017.

[22] Jessica C. E. Irving, Vedran Lekić, Cecilia Durán, Mélanie Drilleau, Doyeon Kim, Attilio Rivoldini, Amir Khan, Henri Samuel, Daniele Antonangeli, William Bruce Banerdt, Caroline Beghein, Ebru Bozdağ, Savas Ceylan, Constantinos Charalambous, John Clinton, Paul Davis, Raphaël Garcia, Domenico Giardini null, Anna Catherine Horleston, Quancheng Huang, Kenneth J. Hurst, Taichi Kawamura, Scott D. King, Martin Knapmeyer, Jiaqi Li, Philippe Lognonné, Ross Maguire, Mark P. Panning, Ana-Catalina Plesa, Martin Schimmel, Nicholas C. Schmerr, Simon C. Stähler, Eleonore Stutzmann, and Zongbo Xu. First observations of core-transiting seismic phases on mars. *Proceedings of the National Academy of Sciences*, 120(18):e2217090120, 2023.

[23] Bruce M. Jakosky and Roger J. Phillips. Mars' volatile and climate history. *Nature*, 412(6843):237–244, Jul 2001.

[24] P.B. James, G.B. Hansen, and T.N. Titus. The carbon dioxide cycle. *Advances in Space Research*, 35(1):14–20, 2005. Mars International Reference Atmosphere, Living With a Star and Fundamental Physics.

[25] Philip B. James, Hugh H. Kieffer, and David A. Paige. The seasonal cycle of carbon dioxide on Mars. In Michael George, editor, *Mars*, pages 934–968. 1992.

[26] F. Y. Jiang, Roger V. Yelle, S. K. Jain, J. Cui, F. Montmessin, N. M. Schneider, J. Deighan, H. Gröller, and L. Verdier. Detection of mesospheric co2 ice clouds on mars in southern summer. *Geophysical Research Letters*, 46(14):7962–7971, 2019.

[27] Jyotirmoy Kalita, Manoj Kumar Mishra, and Anirban Guha. Martian limb-viewing clouds: A study based on mcc, mcs and marci observations. *Planetary and Space Science*, 208:105347, 2021.

[28] D. M. Kass, A. Kleinböhl, D. J. McCleese, J. T. Schofield, and M. D. Smith. Interannual similarity in the martian atmosphere during the dust storm season. *Geophysical Research Letters*, 43(12):6111–6118, 2016.

[29] A.J. Kliore. Radio occultation exploration of mars. *Symposium - International Astronomical Union*, 65:295–316, 1974.

[30] O. Korablev, F. Montmessin, A. Trokhimovskiy, A. A. Fedorova, A. V. Shakun, A. V. Grigoriev, B. E. Moshkin, N. I. Ignatiev, F. Forget, F. Lefèvre, K. Anufreychik, I. Dzuban, Y. S. Ivanov, Y. K. Kalinnikov, T. O. Kozlova, A. Kungurov, V. Makarov, F. Martynovich, I. Maslov, D. Merzlyakov, P. P. Moiseev, Y. Nikolskiy, A. Patrakeev, D. Patsaev, A. Santos-Skripko, O. Sazonov, N. Semena, A. Semenov, V. Shashkin, A. Sidorov, A. V. Stepanov, I. Stupin, D. Timonin, A. Y. Titov, A. Viktorov, A. Zharkov, F. Altieri, G. Arnold, D. A. Belyaev, J. L. Bertaux, D. S. Betsis, N. Duxbury, T. Encrenaz, T. Fouchet, J.-C. Gérard, D. Grassi, S. Guerlet, P. Hartogh, Y. Kasaba, I. Khatuntsev, V. A. Krasnopolsky, R. O. Kuzmin, E. Lellouch,

M. A. Lopez-Valverde, M. Luginin, A. Määttänen, E. Marcq, J. Martin Torres, A. S. Medvedev, E. Millour, K. S. Olsen, M. R. Patel, C. Quantin-Nataf, A. V. Rodin, V. I. Shematovich, I. Thomas, N. Thomas, L. Vazquez, M. Vincendon, V. Wilquet, C. F. Wilson, L. V. Zasova, L. M. Zelenyi, and M. P. Zorzano. The atmospheric chemistry suite (acs) of three spectrometers for the exomars 2016 trace gas orbiter. *Space Science Reviews*, 214(1):7, Nov 2017.

[31] Richard Kruse. Comparison of several mars probes, historic spacecraft. `https://historicspacecraft.com`. Accessed on 02/01/2024.

[32] Takeshi Kuroda, Alexander S. Medvedev, Yasumasa Kasaba, and Paul Hartogh. Carbon dioxide ice clouds, snowfalls, and baroclinic waves in the northern winter polar atmosphere of mars. *Geophysical Research Letters*, 40(8):1484–1488, 2013.

[33] Montabone L. Climatologies of the martian atmospheric dust optical depth. `https://www-mars.lmd.jussieu.fr/mars/dust_climatology/`. Accessed on 02/01/2024.

[34] NASA's Jet Propulsion Laboratory. A mars dust tower stands out. `https://www.jpl.nasa.gov/images/pia23513-a-mars-dust-tower-stands-out`. Accessed on 15/12/2023.

[35] NASA's Jet Propulsion Laboratory. Seasonal temperature pattern indicating martian dust storms. `https://mars.nasa.gov/resources/7851/seasonal-temperature-pattern-indicating-martian-dust-storms/`. Accessed on 05/01/2024.

[36] J. N. Maki, D. Gruel, C. McKinney, M. A. Ravine, M. Morales, D. Lee, R. Willson, D. Copley-Woods, M. Valvo, T. Goodsall, J. McGuire, R. G. Sellar, J. A. Schaffner, M. A. Caplinger, J. M. Shamah, A. E. Johnson, H. Ansari, K. Singh, T. Litwin, R. Deen, A. Culver, N. Ruoff, D. Petrizzo, D. Kessler, C. Basset, T. Estlin, F. Alibay, A. Nelessen, and S. Algermissen. The mars 2020 engineering cameras and microphone on the perseverance rover: A next-generation imaging system for mars exploration. *Space Science Reviews*, 216(8):137, Nov 2020.

[37] D. J. McCleese, J. T. Schofield, F. W. Taylor, S. B. Calcutt, M. C. Foote, D. M. Kass, C. B. Leovy, D. A. Paige, P. L. Read, and R. W. Zurek. Mars climate sounder: An investigation of thermal and water vapor structure, dust and condensate distributions in the atmosphere, and energy balance of the polar regions. *Journal of Geophysical Research: Planets*, 112(E5), 2007.

[38] ESA/ATG medialab. How exomars studies the atmosphere. `https://www.esa.int/ESA_Multimedia/Images/2018/04/How_ExoMars_studies_the_atmosphere`. Accessed on 01/01/2024.

[39] Franck Montmessin, Jean-Loup Bertaux, Eric Quémerais, Oleg Korablev, Pascal Rannou, François Forget, Séverine Perrier, Didier Fussen, Sébastien Lebonnois, Aurélie Rébérac, and Emmanuel Dimarellis. Subvisible co2 ice clouds detected in the mesosphere of mars. *Icarus*, 183(2):403–410, 2006.

[40] A. Määttänen, F. Montmessin, B. Gondet, F. Scholten, H. Hoffmann, F. González-Galindo, A. Spiga, F. Forget, E. Hauber, G. Neukum, J.-P. Bibring, and J.-L. Bertaux. Mapping the mesospheric co2 clouds on mars: Mex/omega and mex/hrsc observations and challenges for atmospheric models. *Icarus*, 209(2):452–469, 2010.

[41] Mark I. Richardson and Michael A. Mischna. Long-term evolution of transient liquid water on mars. *Journal of Geophysical Research: Planets*, 110(E3), 2005.

[42] R. S. Saunders, R. E. Arvidson, G. D. Badhwar, W. V. Boynton, P. R. Christensen, F. A. Cucinotta, W. C. Feldman, R. G. Gibbs, C. Kloss, M. R. Landano, R. A. Mase, G. W. McSmith, M. A. Meyer, I. G. Mitrofanov, G. D. Pace, J. J. Plaut, W. P. Sidney, D. A. Spencer, T. W. Thompson, and C. J. Zeitlin. 2001 mars odyssey mission summary. *Space Science Reviews*, 110(1):1–36, Jan 2004.

[43] J T Schofield, J R Barnes, D Crisp, R M Haberle, S Larsen, J A Magalhães, J R Murphy, A Seiff, and G Wilson. The mars pathfinder atmospheric structure investigation/meteorology (ASI/MET) experiment. *Science*, 278(5344):1752–1758, December 1997.

[44] Cem Berk Senel, Orkun Temel, Christopher Lee, Claire E. Newman, Michael A. Mischna, Domingo Muñoz-Esparza, Hakan Sert, and Özgür Karatekin. Interannual, seasonal and regional variations in the martian convective boundary layer derived from gcm simulations with a semi-interactive dust transport model. *Journal of Geophysical Research: Planets*, 126(10):e2021JE006965, 2021. e2021JE006965 2021JE006965.

[45] M. Slipski, B. M. Jakosky, M. Benna, M. Elrod, P. Mahaffy, D. Kass, S. Stone, and R. Yelle. Variability of martian turbopause altitudes. *Journal of Geophysical Research: Planets*, 123(11):2939–2957, 2018.

[46] Paul M. Streeter, Stephen R. Lewis, Manish R. Patel, James A. Holmes, and David M. Kass. Surface warming during the 2018/mars year 34 global dust storm. *Geophysical Research Letters*, 47(9):e2019GL083936, 2020. e2019GL083936 2019GL083936.

[47] Orkun Temel, Özgür Karatekin, Michael A. Mischna, Cem Berk Senel, Germán Martínez, Elodie Gloesener, and Tim Van Hoolst. Strong seasonal and regional variations in the evaporation rate of liquid water on mars. *Journal of Geophysical Research: Planets*, 126(10):e2021JE006867, 2021. e2021JE006867 2021JE006867.

[48] Ann Carine Vandaele, Oleg Korablev, Frank Daerden, Shohei Aoki, Ian R. Thomas, Francesca Altieri, Miguel López-Valverde, Geronimo Villanueva, Giuliano Liuzzi, Michael D. Smith, Justin T. Erwin, and et al. Martian dust storm impact on atmospheric h2o and d/h observed by exomars trace gas orbiter. *Nature*, 568(7753):521–525, Apr 2019.

[49] Paul Withers, M. Felici, M. Mendillo, L. Moore, C. Narvaez, M. F. Vogt, K. Oudrhiri, D. Kahan, and B. M. Jakosky. The maven radio occultation science experiment (rose). *Space Science Reviews*, 216(4):61, May 2020.

[50] R. Wordsworth, F. Forget, E. Millour, J.W. Head, J.-B. Madeleine, and B. Charnay. Global modelling of the early martian climate under a denser co2 atmosphere: Water cycle and ice evolution. *Icarus*, 222(1):1–19, January 2013.

[51] Zhaopeng Wu, Mark I. Richardson, Xi Zhang, Jun Cui, Nicholas G. Heavens, Christopher Lee, Tao Li, Yuan Lian, Claire E. Newman, Alejandro Soto, Orkun Temel, Anthony D. Toigo, and Marcin Witek. Large eddy simulations of the dusty martian convective boundary layer with marswrf. *Journal of Geophysical Research: Planets*, 126(9):e2020JE006752, 2021. e2020JE006752 2020JE006752.

[52] Richard W. Zurek and Suzanne E. Smrekar. An overview of the mars reconnaissance orbiter (mro) science mission. *Journal of Geophysical Research: Planets*, 112(E5), 2007.

UNIVERSITÉ CATHOLIQUE DE LOUVAIN
Faculté des sciences
Place des sciences, 2 bte L6.06.01, 1348 Louvain-la-Neuve, Belgique | **www.uclouvain.be/sc**